Journal of Sound and Vibration (2002) **257**(3), 527–557
doi:10.1006/jsvi.5051, available online at http://www.idealibrary.com on IDEAL®

THE INFLUENCE OF CYLINDER LUBRICATION ON PISTON SLAP

S. N. Y. Gerges

Noise and Vibration Laboratory, Mechanical Engineering Department, Federal University of Santa Catarina, Cx.P. 476, *CEP:* 88040-900, *Florianopolis, SC, Brazil. E-mail: samir@emc.ufsc.br*

J. C. de luca

*RENAULT—Driveline NVH, CLT L*23 1 45, 1, *Allee Cornuel,* 91510, *Lardy, France*

AND

N. Lalor

*Institute of Sound and Vibration Research, The University of Southampton, Highfield, Southampton, SO*17 1*BJ, England*

(*Received* 21 *November* 2000, *and in final form* 14 *January* 2002)

A model has been developed for determining the time history of piston slap impact force. This model takes into account the influence of the oil film on the impact behaviour, which was found to be an important factor. However, it was also found that entrapped gas bubbles in the oil are equally significant. Three test rigs were designed and built to study these effects on the impact phenomenon and extensive tests were carried out. The impact force time history has been determined using Reynolds' theory. Results have shown that Reynolds' theory for fluid film squeezing can be applied for oil film damping determination. However, the experimental results have also shown that when gas is entrapped during the impact, this theory considerably overpredicts the magnitude of the impact. An eight-degree-of-freedom lumped parameter model was developed through the dynamic analysis of each component of an internal combustion engine's reciprocating system. The effective damping factor derived from this model was found to be inversely proportional to the oil film thickness cubed, as expected from Reynolds' theory. A dynamic model has been proposed, where the oil film mixed with bubbles is considered to be analogous to a serial spring and damping system. By incorporating a spring in series with this damper, the effect of the bubbles can also be predicted.

1. INTRODUCTION

The two main noise sources of an engine are the combustion process and mechanical impacts. Of the latter, generally the most important is piston slap [1–17], which is produced by impacts between the piston and cylinder wall. These impacts cause the engine outer surfaces to vibrate and consequently radiate noise.

In order to control engine noise, it is important to understand and measure piston slap. Many models have been developed to measure and/or predict this source of noise [17–24], and most of the recent models have considered the influence of the oil film on this type of

0022-460X/02/$35.00

impact. This work presents a study of the influence of a lubricant on piston slap and analyses the precision of Reynolds' theory for determining its force time history.

This research has been carried out by supporting each stage in the analytical formulation by experimental tests on specially constructed test rigs. The project was divided into three stages, as follows:

Stage I: An extensive study of the influence of the oil film on the impact behaviour of two rigid bodies was carried out using a specially designed test rig. The measured impact forces were compared with calculated values using an analytical equation derived from Reynolds' theory.

Stage II: The impacts between piston and cylinder wall were studied on a second test rig that was constructed using a specially adapted 1·8 l diesel engine block. These experimental impact tests were much closer to the real impacts in an engine. An eight-degree-of-freedom (d.o.f.) lumped parameter model was developed using the dynamic characteristics of the piston, connecting rod, cylinder wall and engine block. The impact force between piston and cylinder wall was determined by means of three calculations utilizing Reynolds' theory, transfer functions and the piston's inertial force.

Stage III: A facility was set-up to motor a fully assembled Diesel engine, nominally identical to the one used in the rig in stage II, at speeds up to 4000 r.p.m. The time history of the piston slap force was determined using the methodologies of stage II for different operational regimes of the engine, and the spectra of the force were compared. These results led to the development of a dynamic model for the impact force which included an oil film mixed with air bubbles.

2. INFLUENCE OF THE OIL FILM ON TWO IMPACTING RIGID BODIES—STAGE I

The influence of an oil film on the impact between two rigid bodies was determined in two ways: using an equation derived from Reynolds' theory for fluid film squeeze and experimentally. Figure 1 shows a schematic diagram of the test rig built for this purpose, where the upper mass is designed to slide freely down the rod and to strike the oil film only with the surface S (an annular ring with inner radius r_1 and outer r_2). This design avoided the effect of the oil meniscus around the rod base, which would otherwise restrict the oil flow at impact. A special case of Reynolds' equation for pure squeezing of a thin film

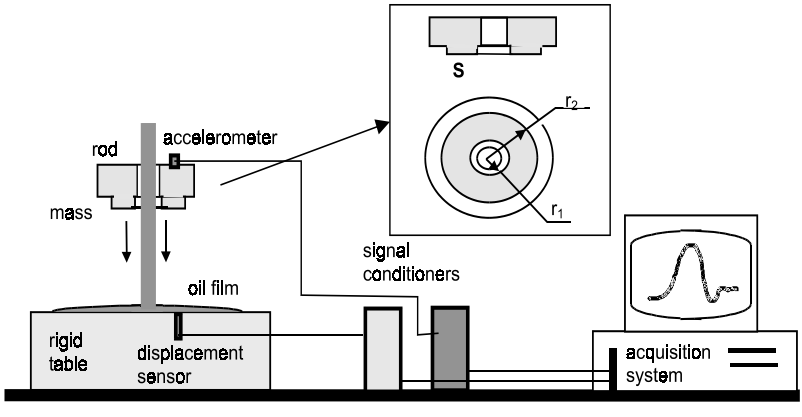

Figure 1. Test rig for generating impacts between two rigid bodies.

between two axisymmetric rigid bodies, assuming that the inertia effects are negligible, is given by [25, 26]

$$\frac{1}{r}\frac{\partial}{\partial r}\left(rh^3\frac{\partial p}{\partial r}\right) = 12\eta v, \tag{1}$$

where p is the fluid film pressure, η the dynamic viscosity, v the relative squeezing velocity and h the fluid film thickness.

For the case of the test rig described in Figure 1, h is constant over the contact surface **S**, and the pressure gradient is zero at $r = r_o$ (radius for maximum pressure). Equation (1) is integrated to obtain the oil pressure distribution in the oil film:

$$r\frac{\partial p}{\partial r} = \int 12\eta v\frac{r}{h^3}\,\mathrm{d}r + A,$$

where A is the integration constant. Since the pressure distribution is continuous over the impact surfaces, there is a radius r_0 where the pressure is maximum, therefore

$$\left.\frac{\partial p}{\partial r}\right|_{r=r_0} = 0, \quad A = -\frac{6\eta v}{h^3}(r_0^2).$$

Using the above condition, the derivative of the pressure with the radius is obtained as

$$\frac{\mathrm{d}p}{\mathrm{d}r} = \frac{6\eta v}{h^3}\left(r - \frac{r_0^2}{r}\right). \tag{2}$$

Equation (2) is integrated to obtain the pressure distribution over the radius r:

$$p(r) = \frac{6\eta v}{h^3}\left[\frac{r^2}{2} - r_0\ln(r) + B\right]. \tag{3}$$

The radius r_0 and the integration constant B are determined using the boundary conditions $p(r_1) = p(r_2) = 0$, resulting in

$$r_0^2 = \frac{(r_2^2 - r_1^2)}{2\ln(r_2/r_1)}, \quad B = r_0^2\ln(r_1) - \frac{r_1}{2}.$$

Substituting for B and r_0 in equation (3) gives

$$p(r) = \frac{3\eta v(r^2\ln(r_2/r_1) + r_2^2\ln(r_1/r) - r_1^2\ln(r_2/r))}{h^3\ln(r_2/r_1)}. \tag{4}$$

The impact force F is determined by integrating the oil film pressure (equation (4)) over the **S** surface:

$$F = \int_{\mathbf{S}} P\,\mathrm{d}S, \quad 2\pi r\,\mathrm{d}r, \tag{5}$$

$$F = \frac{3\eta\pi v}{h^3}\frac{(r_2^4(\ln(r_2/r_1) - 1) + 2r_2^2r_1^2 - r_1^4(\ln(r_2/r_1) + 1))}{2\ln(r_1/r_2)}, \tag{6}$$

where F is the resultant squeeze force acting on the mass during the impact. F has the character of a viscous force; $F_{VISCOUS} = C_0 v$ where C_0 is the effective damping factor.

The effective damping factor can be defined from equation (6) as

$$C_0 = \frac{3\eta\pi}{h^3}\frac{(r_2^4(\ln(r_2/r_1) - 1) + 2r_2^2r_1^2 - r_1^4(\ln(r_2/r_1) + 1))}{2\ln(r_1/r_2)}. \tag{7}$$

Equation (7) shows that the effective damping factor is inversely proportional to the oil film thickness to the power three, and directly proportional to the viscosity. A geometrical

factor (*ffact*) can be defined from equation (7). This factor depends exclusively on the geometry of the impacting surfaces, and in this case is

$$ffact = 3\pi \frac{(r_2^4(\ln(r_2/r_1) - 1) + 2r_2^2r_1^2 - r_1^4(\ln(r_2/r_1) + 1))}{2\ln(r_1/r_2)}.$$

A general expression can be written for the impact force as

$$F = \frac{\eta v}{h^3} ffact.$$

The test rig was set-up with an eddy current displacement sensor and an accelerometer attached to the upper mass. The output from each measuring system was fed in a PC-based acquisition card. All data acquisitions were pre-triggered by the displacement sensor when the mass was around 400 m from the table surface, and simultaneous acceleration and displacement signals were automatically measured. An oil, 15W40, was used for all tests, the viscosity of which was determined by means of a sphere viscometer in the temperature range of 20–40°C. These results enabled the following expression to be derived:

$$\eta(T) = 0{\cdot}94e^{-0{\cdot}057T} \quad \text{(Pa s)}, \tag{8}$$

where T is the oil temperature (°C).

Prior to each impact, an oil film of nominal thickness was spread on the table by releasing a known quantity of oil and measuring the diameter of spread. The mass was then released from a given height and the above measurements were taken. This procedure was repeated for different oil film thicknesses and mass drop heights. Thus, for each test a continuous time record of force on the mass (moving mass times its acceleration = experimental F, see Figure 2, top left curve), velocity of the mass (see Figure 2, lower right curve)

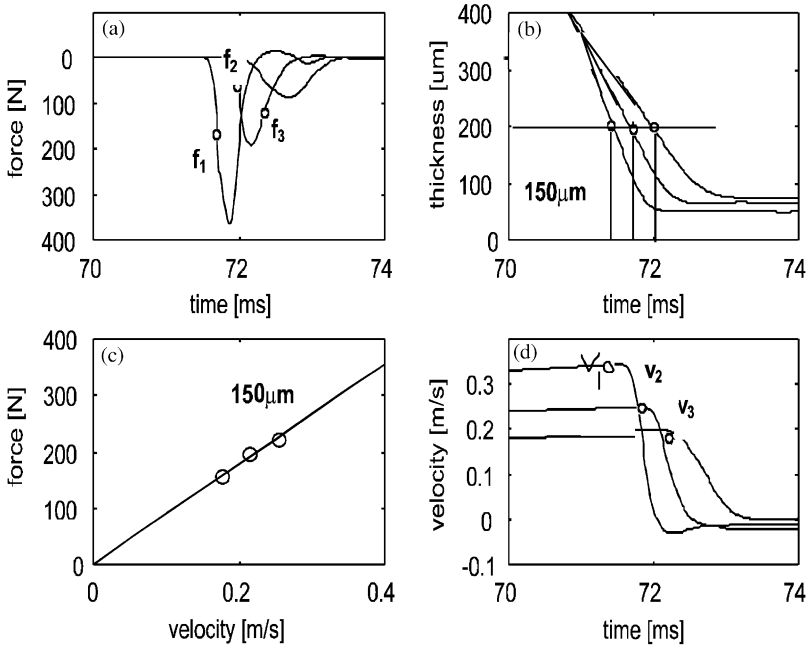

Figure 2. Force on mass versus velocity for oil film thickness 150 μm: (a) force versus time, (b) thickness versus time, (c) force versus velocity, (d) velocity versus time.

and oil film thickness (displacement signal (h)—see Figure 2, upper left curve) was obtained during the impact. The initial thickness of the oil film (at the moment when the upper mass touches the oil) can be found from the value of the displacement signal at the moment the acceleration suddenly changes direction. By combining the results from all these tests, it was possible to select points where the oil film thickness was the same but the velocity of the mass (and hence, the force on the mass) was different. This force was then plotted against the corresponding velocity for a given oil film thickness (as shown in Figure 2—lower left). It should be emphasized that the thickness referred to is not the initial value but the value at the instant when the velocity and force were selected. The data points are shown in Figure 3 and are very close to the best-fit lines using the least-squares method. This indicates that, for constant thickness h, the force is proportional to velocity, as would be expected from equation (6). It was also observed that these lines do not go through the origin, which means that there is a small residual force on the mass at zero velocity. Up to this point, it had been established that the oil behaved essentially as a Newtonian fluid and that Reynolds' theory was qualitatively applicable. The next step was therefore to determine whether equation (6) could predict the absolute level of the impact force. Initially, very poor agreement was obtained, especially for high-velocity impacts where the Reynolds' force was up to an order of magnitude higher than the measured value. The problem was traced to the fact that tiny air bubbles were forced into the oil cushioning the impact, greatly reducing the peak force and the oil film carrying capacity [27, 28]. By removing the mass just after the impact, these bubbles could be seen trapped in the oil film. These air bubbles are pushed into the oil film by the moving mass, when the air does not have enough time to escape just before the impact takes place. The air viscosity at 20°C is around 17 000 times lower than the viscosity of the 15W40 oil, which means that a very small number of air bubbles can significantly change the effective viscosity [29]. As stated above, the force calculated using equation (6) may be an order of magnitude higher than that obtained experimentally (Figure 4).

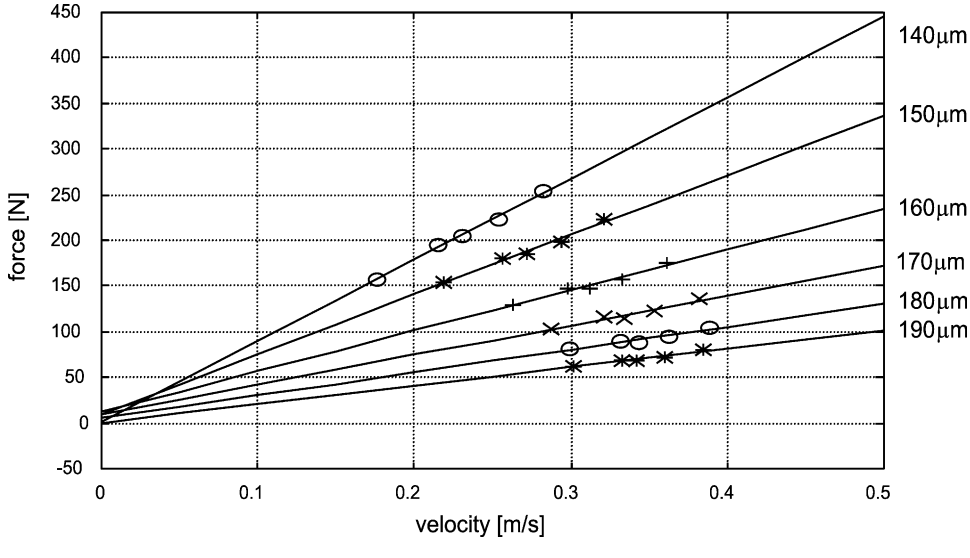

Figure 3. Curves of force versus velocity for known oil film thickness, experimental points and best-fit line using least-squares method.

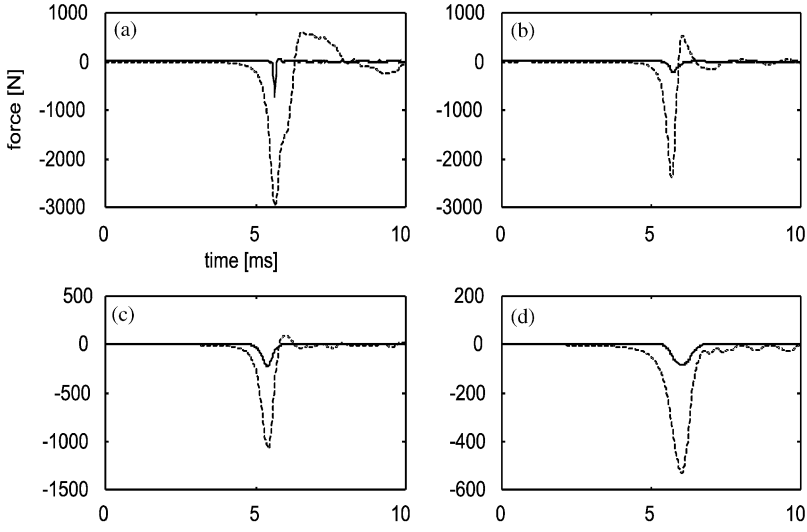

Figure 4. Impact force time histories: experimental (- - -) and calculated from equation (6) (——), before reducing air trapped, for different drop hights: (a) 100 mm, (b) 85 mm, (c) 70 mm and (d) 55 mm.

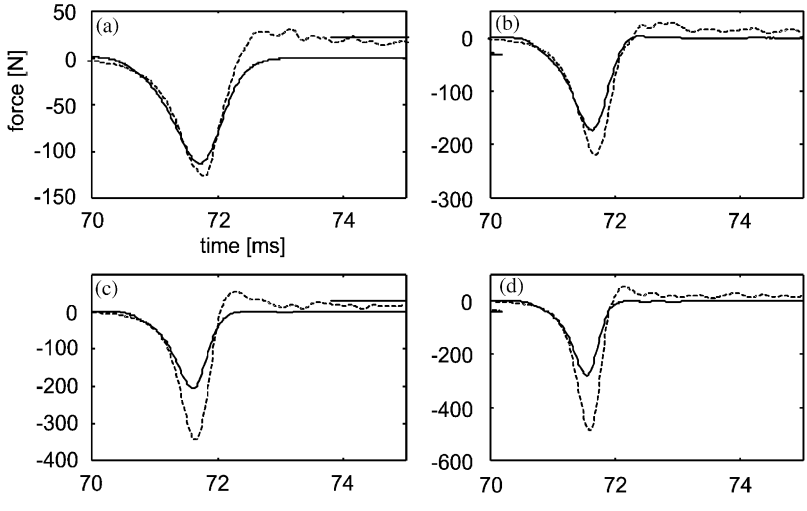

Figure 5. Impact force time histories: experimental (- - -) and calculated from equation (6) (——), after reducing air trapped, for different drop hights: (a) 55 mm, (b) 70 mm, (c) 85 mm and (d) 100 mm.

Spreading a layer of oil over the mass surface reduces drastically the formation of air being entrapped. Figure 5 shows a typical comparison between measured (mass $\times$ acceleration) and calculated (equation (6)) impact force time histories, after this modification has been carried out (spreading oil over the mass). It was observed that the higher the impact velocity, the higher the disagreement between calculated and measured forces, and that the error was greater for thinner oil films. It is suggested that the quantity of air trapped is directly proportional to the following parameters: initial impact velocity, surface area of impact and impact surface form.

An empirical equation has been proposed to determine the ratio between the peak force obtained from equation (6) and the measured force. This equation has been determined using 25 different impact configurations, with the initial oil film thickness from 100 to 500 m and impact velocities from 0·1 to 0·4 m/s. The ratios were related to the film thickness (h) and impact velocity (v) by the general equation $Ave^{\alpha h}$, where A and α are constants related to the surface area and form, and characteristics of the oil. The least-squares method was used to find the best fit for the coefficients A and α, and the resultant equation is

$$ratio = 75ve^{-5210h}, \tag{9}$$

where *ratio* is the peak (analytical force)/peak (measured force), v the initial impact velocity (m/s) and h the initial oil film thickness (m).

The effective damping factor for a given thickness is obtained from the slope of each fitted line. Figure 6 shows the effective damping factor points plotted versus the respective oil film thickness (obtained from Figure 3 using the least-squares method power best-fit curve), which can be expressed as

$$C_0 = \frac{8 \times 75 \times 10^8}{h^{2.8}} \text{(Ns/m)}, \tag{10}$$

where h is the oil film thickness in (m).

Equation (10) implies that the effective damping factor is inversely proportional to the film thickness to the power of 2·8, which is close to the theoretical value of 3·0 of equation (7). This can be a useful empirical formula for predicting the type of oil used.

3. INFLUENCE OF THE OIL FILM ON THE IMPACT BETWEEN PISTON AND CYLINDER WALL—STAGE II

The influence of an oil film on the impact between piston and cylinder wall (piston slap) was also determined using a finite difference form of Reynolds' theory and experimentally measured in three ways, using a specially designed and built test rig.

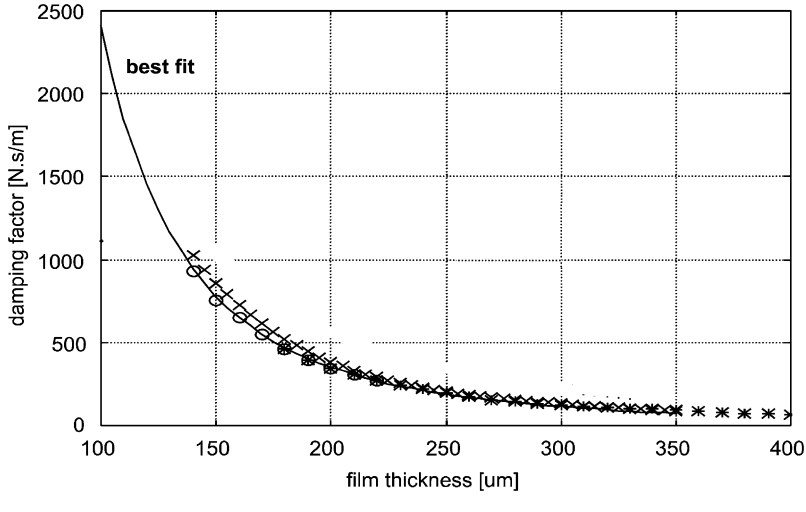

Figure 6. Oil-damping factor as a function of thickness (×, *, and 0 are experimental data).

3.1. TEST RIG DESIGN

In order to proceed with the experimental tests, a second rig was constructed from an engine block specially modified for the purpose (Figure 7). The crank-shaft was fitted with the big end at the TDC position at the test cylinder and clamped to the main bearing caps. A connecting rod and piston were also installed. The profile of the piston was carefully measured using a TALYROND 200 roundness meter. It was assumed that the cylinder profile was perfectly cylindrical. Although this was not strictly accurate, it was considered likely that the piston profile would have a much greater effect on piston/cylinder gap variation than cylinder distortion. Therefore, the latter could be safely ignored. Two grub screws (jet screws) were fitted to the small end so that the angle between the piston and connecting rod could be locked at known angles (see Figure 8). The cut-away section of the cylinder enabled the piston to be dropped from different heights, allowing the generation of piston impact velocities representative of the running engine.

Two eddy current displacement transducers were installed in the wall of the cylinder along the thrust line, and flush with its inner surface (ds_1 and ds_2). They were positioned to measure the displacements of the top and bottom of the piston skirt. Accelerometers were placed at the small end (*ase*), on the piston skirt (*ads* and *ats*), on the outer cylinder wall (*acw*) and on a point on the outer wall of the engine block (Figure 8). A thin film of oil was then smeared onto the cylinder wall and the piston quickly dropped before the oil had time to flow down the sides. Many different impact configurations (velocity and oil film thickness) could then be generated. The data from all the sensors were simultaneously recorded at a sampling frequency of 32·7 kHz, over a period of 15·6 ms during the impact. The acquisitions were pre-triggered by the displacement sensor ds_2, when the piston's bottom skirt was 400 μm from the cylinder wall.

A lumped parameter model of the system composed of connecting rod, piston and cylinder wall (plus the rest of the engine block) was proposed [28] for the engine. This model (Figure 9) was obtained after a dynamic analysis of each component up to frequencies of 5 kHz. A modal analysis was performed on the piston which showed that,

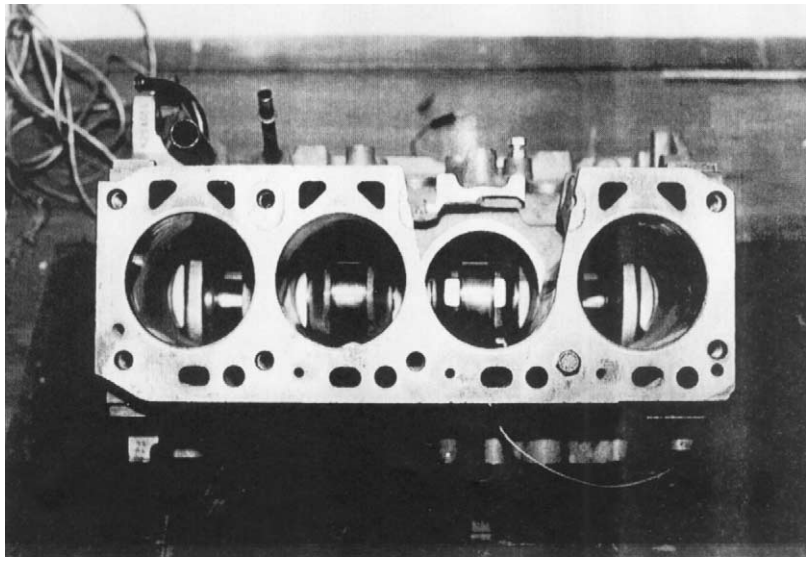

Figure 7. Engine block modified for impacting tests.

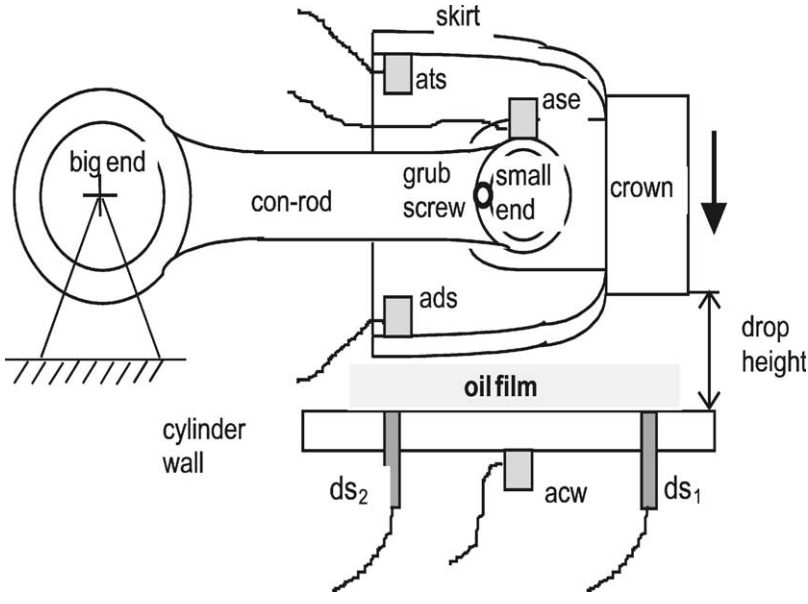

Figure 8. Instrumentation of the second test rig.

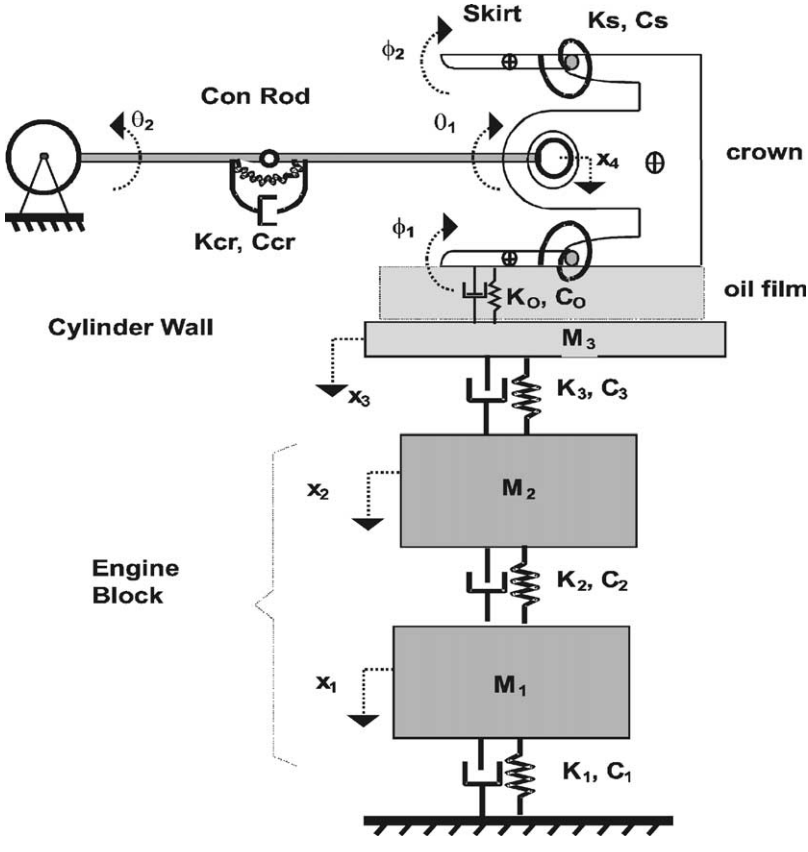

Figure 9. Lumped parameter model.

up to 5 kHz, there are two modes where the skirts deflect practically linearly. This suggests that, in the two-dimensional plane of the figure, the piston skirts can be modelled as rigid bars pivoted about the crown. The cylinder wall plus engine block were represented by a 3-d.o.f. system, and the first bending mode of the connecting rod has been considered. With the exception of the oil's damping factor (*Co*), all parameters in this lumped parameter model are constant. Therefore, a dynamic equilibrium equation can be written and solved for *Co* by the central difference method, using the acquired data for each impact generated.

The dynamic matrices of this system were reduced to 7 d.o.f. by locking the degree of freedom θ_1 using a grub screw fitted at the small end. The elements in each matrix were obtained by curve fitting of the experimental frequency response curves measured in each sub-system. After some impacts with low squeeze velocities, it was observed that the residual oil film stiffness can be neglected ($Ko \approx 0$).

3.2. APPLICATION OF REYNOLDS THEORY TO ASSESS PISTON IMPACTING FORCE

Clearly, in this case no simple equation (as that for the first rig) could be derived to calculate the impact force. Instead, the lower half of the piston skirt surface was divided into small elements (Figure 10). By knowing the top and bottom skirt displacements and the profiles of the piston skirt and cylinder wall, the time history of the piston/cylinder clearance $h(t)$ was determined. These time histories were used to solve the finite difference form of Reynolds' equation in cylindrical co-ordinates, giving as a result the impact force time history (F_{Re}) in each section of the mesh.

The connecting rod was connected to the crank-shaft with very reduced lateral clearance to prevent the piston moving sideways during the impact. The oil film thickness between piston skirt and cylinder wall surfaces was obtained by combining their profiles and considering their spatial orientation. An example of the discretized oil film thickness over the surfaces is shown in Figure 11.

The impacting surfaces were divided into $\mathbf{n} \times \mathbf{m}$ square parts and the oil pressure was considered to be zero at the boundaries of the impacting surfaces, where there is no oil. Figure 12 shows the results of impact force calculated by using different mesh sizes, such as 2×2, 5×5, 8×8 and $10 \times 10\,\text{mm}^2$, with a total surface of integration of $40 \times 40\,\text{mm}^2$ and same thickness time history and oil film viscosity. The graphs in this figure are

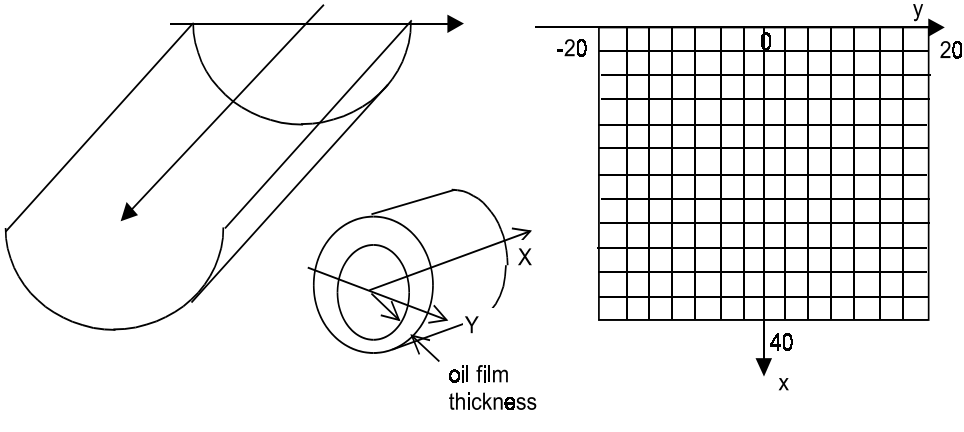

Figure 10. Impacting surfaces meshed into sub-areas.

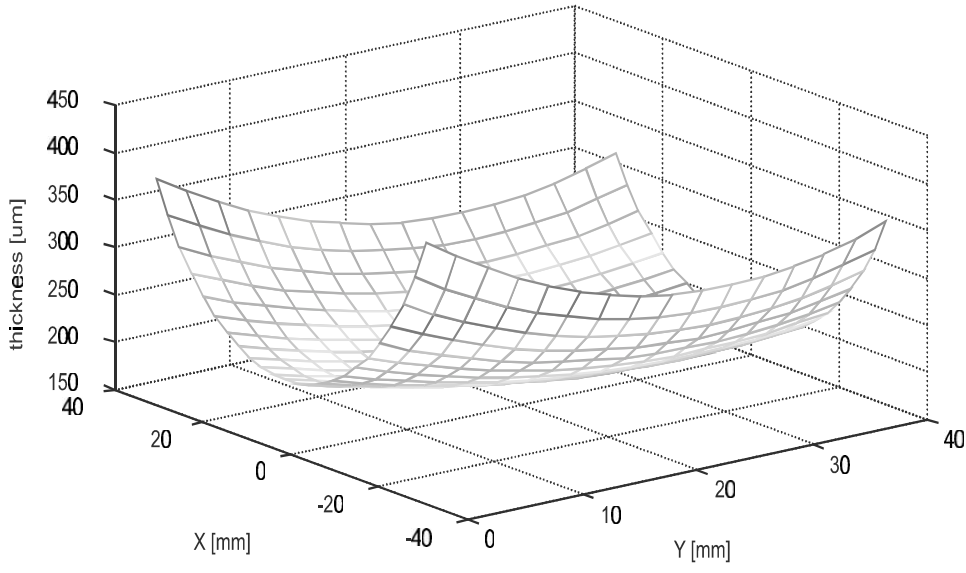

Figure 11. Oil film thickness over the impacting surfaces.

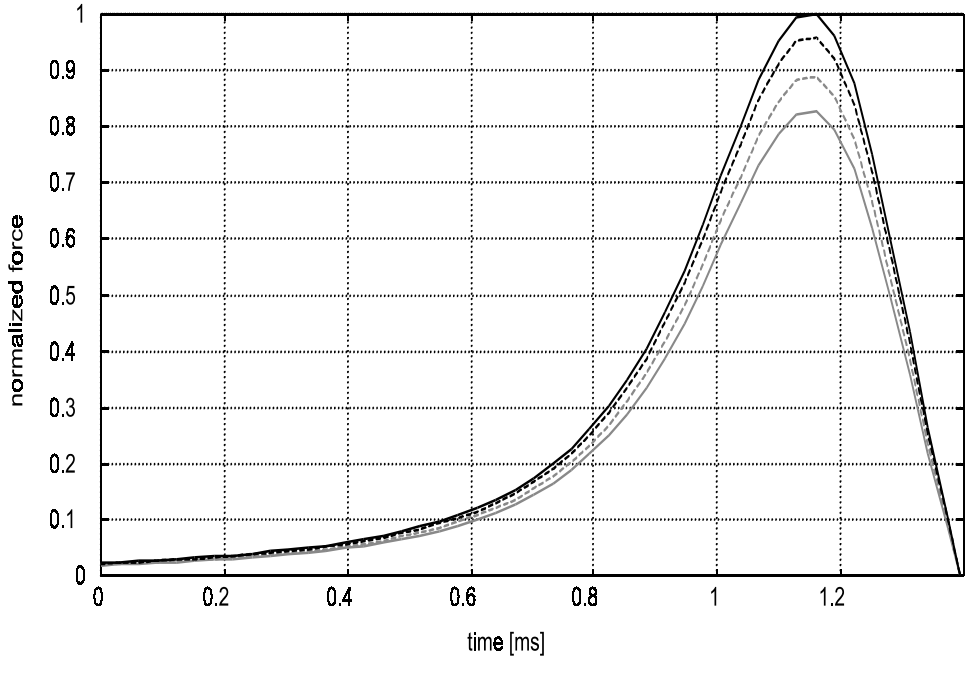

Figure 12. Normalized forces time history for different mesh sizes. From top to bottom: 2×2, 5×5, 8×8 and $10 \times 10\,\text{mm}^2$, with a surface of integration of $40 \times 40\,\text{mm}^2$.

normalized to the maximum calculated value to give an idea of the variation of the maximum force due to the surfaces' meshing. The computer (Pentium 200 with 32 Mb RAM) and mathematical software (MatLab 4·0) could not solve the integration for

meshes with sizes smaller than $1{\cdot}5 \times 1{\cdot}5\,\text{mm}^2$ and an integration surface of $40 \times 40\,\text{mm}^2$. Figure 12 shows that when the mesh is refined, the integrated impact force increases more slowly. It was observed that the $5 \times 5\,\text{mm}^2$ mesh size gave a result only 4% lower than the $2 \times 2\,\text{mm}^2$ mesh. The number of equations to be solved for the $5 \times 5\,\text{mm}^2$ mesh is 49 while for the $2 \times 2\,\text{mm}^2$ mesh is 361. Figure 13 shows a typical pressure distribution over the impacting surfaces using a $2 \times 2\,\text{mm}^2$ mesh.

The squeezing pressure is integrated over the impacting surfaces to obtain the impact force. For the case shown in Figure 13, resultant force of 1900 N is obtained. These calculations are carried out for each time step during the impact, and the final result is the impact force time history.

3.3. EXPERIMENTAL TESTS

The experimental tests consisted basically of producing different configurations of the impact between piston and cylinder wall. These configurations are defined by the locked angle of the piston, the initial oil film thickness and impact velocity. The test steps for each configuration are: the piston angle is adjusted and locked using two grub screws, a known volume of oil is spread over the cylinder wall and a thin layer over the piston skirt. Then, an impact velocity is generated by lifting and releasing the piston from a height.

The piston was locked at angles of $-0{\cdot}14$, $-0{\cdot}07$, $0{\cdot}00$ and $0{\cdot}04^\circ$, and the clockwise direction, as viewed from the front of the engine, was adopted as a positive angle (Figure 14).

For a selected angle, a variation of $\pm 0{\cdot}01^\circ$ was observed after many impacts. For each angle, the piston was released from five different heights. For each height three different oil volumes were spread over the cylinder wall, generating nominal oil film thickness between 200 and 400 µm. Although these are greater than in a running engine (normally less than 50 m), it would be quite difficult to generate and control the correct values. However, because the purpose of this test rig is to assess the calculation model, these greater thicknesses are acceptable.

The nominal oil film thickness is obtained experimentally by determining the first moment when the bottom skirt acceleration *ads* (Figure 8) changes its direction from

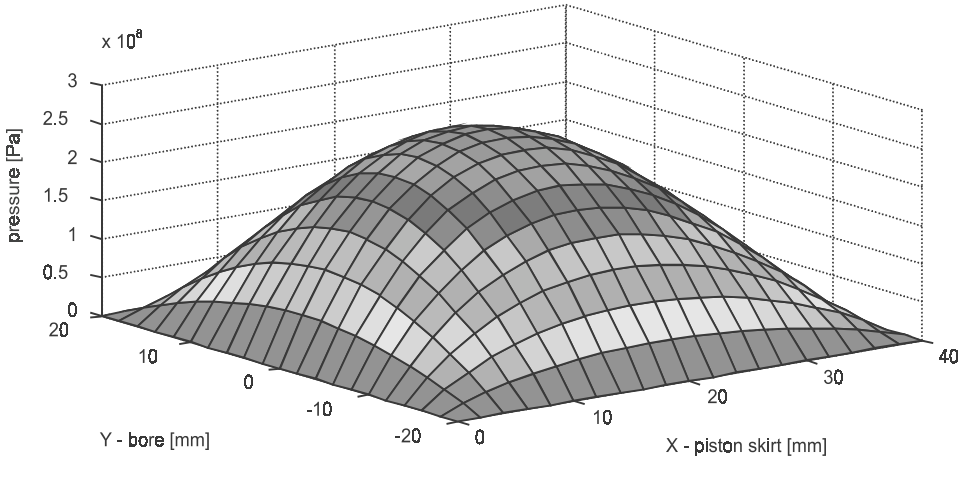

Figure 13. Pressure distribution for one impact moment and mesh size $2 \times 2\,\text{mm}^2$.

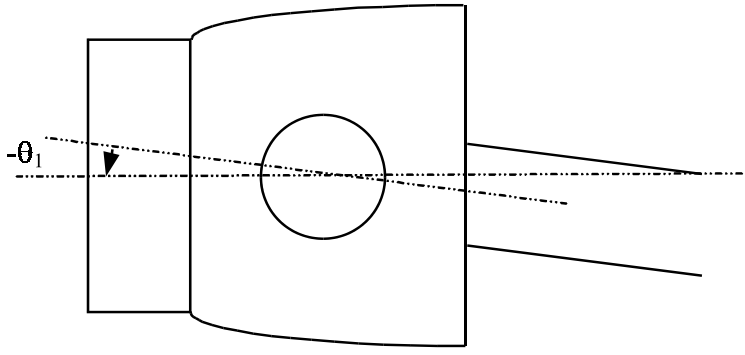

Figure 14. Piston tilt angle.

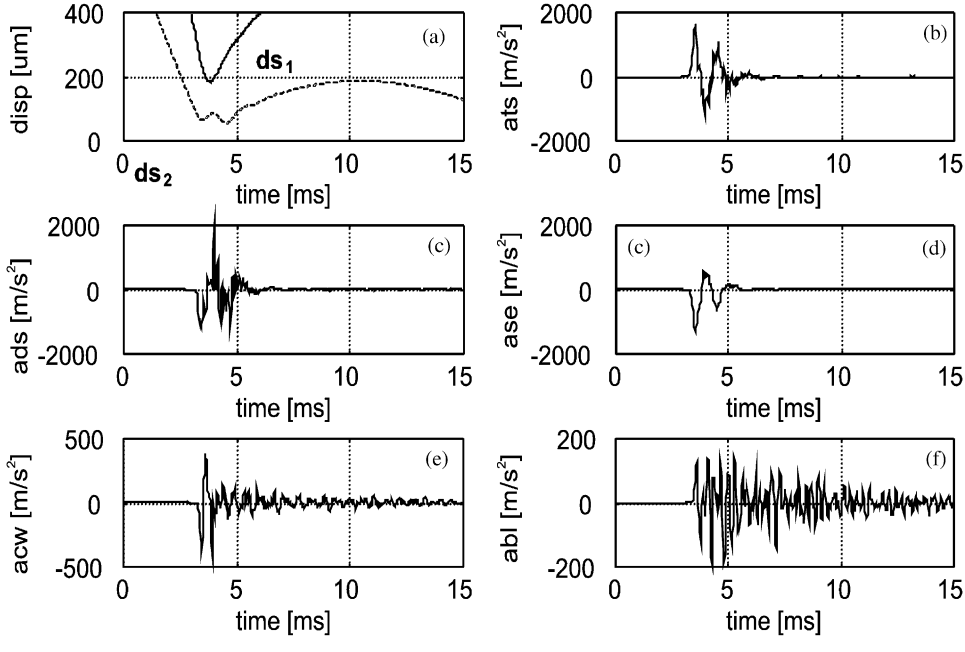

Figure 15. Typical experimental measurements of (a) ds_1 and ds_2, (b) *ats*, (c) *ads*, (d) *ase*, (e) *acw* and (f) *abl* (engine block).

positive to negative (considered as the start of the impact). A time sample history for all quantities acquired on each impact generated is shown in Figure 15. The temperature of the cylinder wall was monitored during all tests in order to determine the oil viscosity using equation (8).

3.3.1. *The measurements*

Before the experimental tests were carried out, some preliminary verifications were done, such as piston print (impact area), piston skirt oscillation (to check if it behaves as a rigid bar) and calibration of all sensors used.

Because the squeeze pressure obtained by using Reynolds theory is highly dependent on the fluid film thickness, which can be affected by the elastic deformations of the cylinder wall and piston skirt, the piston skirt oscillations were checked. The amplitude of these oscillations was determined using the experimental measurements of the piston skirt displacements.

An oscillation of the skirt was also observed at a frequency of about 650 Hz, which is the natural frequency of the piston rotation about the small end, with the grub screws acting as torsional springs. Figure 16 shows the drive-point inertance for the assembly piston and connecting rod with the grub screws loose and locked. The fact that each side of the piston skirt could be considered as a rigid body has been confirmed by Ohta *et al.* [4].

The average temperature for all tests was $20{\cdot}0 \pm 1{\cdot}0°C$, giving an oil viscosity of $0{\cdot}29 \pm 0{\cdot}02$ Pa s. The experimental measurements were carried out following the previously presented procedure. Sixty different impacts were generated, and for each impact seven time histories were measured.

3.3.2. *Data processing and analysis*

The experimental data were processed in order to obtain the impact force time history (piston slap) in four different ways:

A. Using the transfer function method: The impact force spectrum was obtained using the transfer function measured at the cylinder wall where the accelerometer *acw* was installed. The engine block can be considered as a linear system, therefore reciprocity and superposition principles apply [30], and the piston slap is the only force that is applied to the structure during each impact. Therefore, the force spectrum is obtained by dividing the acceleration spectrum of *acw* by the drivepoint inertance (Figures 17 and 18).

B. Using the small end acceleration. The effective impacting mass is the sum of the masses of the whole piston, gudgeon pin and effective small end mass (which for this system is 0·93 kg). By multiplying this mass by the small end acceleration (ase), the impact

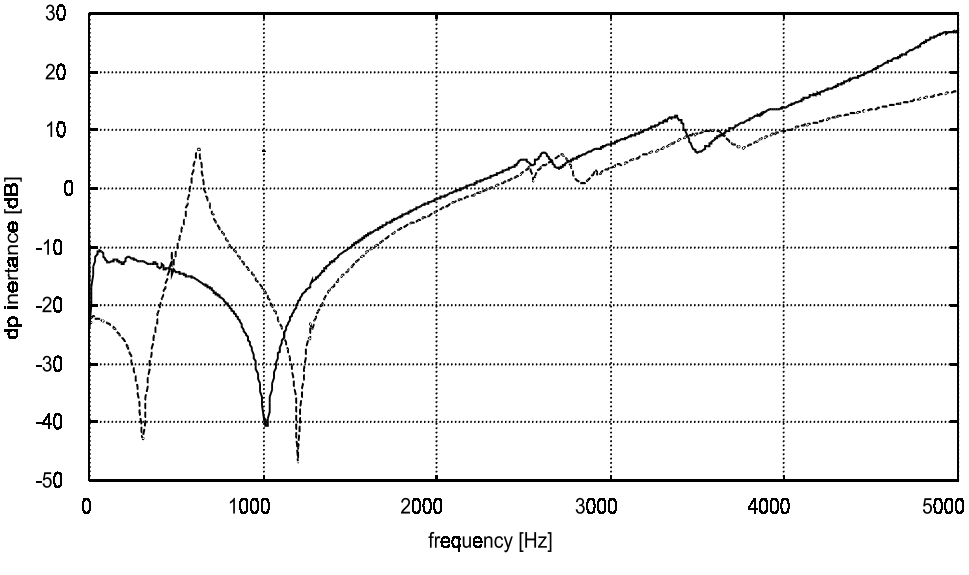

Figure 16. Drive-point inertia at middle skirt of piston free (——) and locked (- - -).

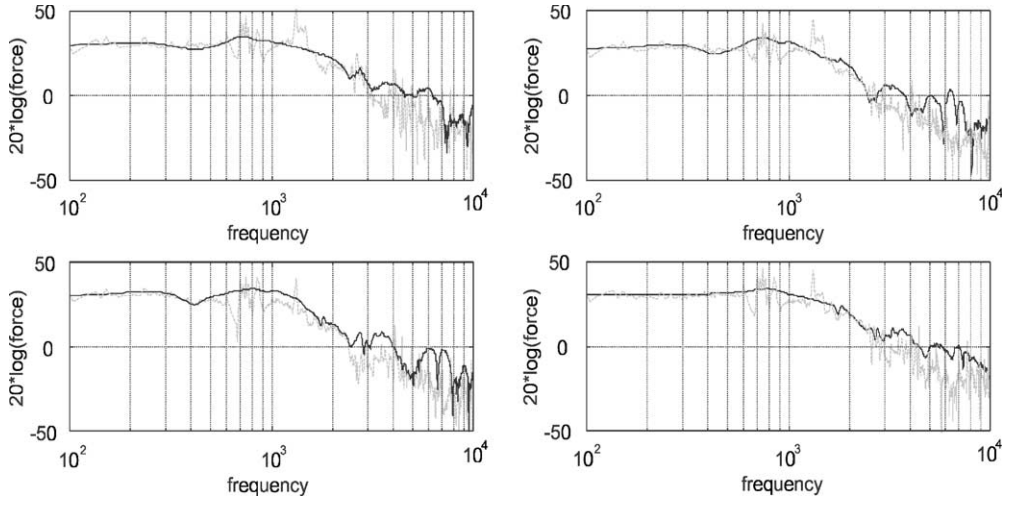

Figure 17. Impact force spectra for the angle of $-0{\cdot}14^\circ$ derived from the transfer function (faint line) and from the small end acceleration (bold line), repeated four times.

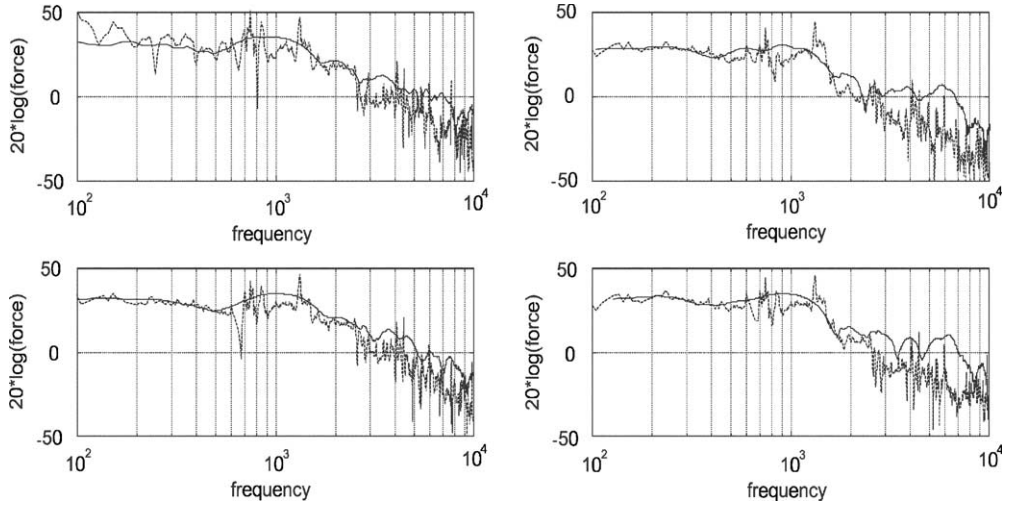

Figure 18. Impact force spectra for the angle of $+0{\cdot}04^\circ$ derived from the transfer function (faint line) and from the small end acceleration (bold line), repeated four times.

force spectrum can be estimated. The results for eight different impact configurations are shown in Figures. 17 and 18, which are related to piston and connection-rod angles of $-0{\cdot}14^\circ$ and $0{\cdot}04^\circ$, with four repetitive trials each. Good agreement between the force spectra obtained using methods A and B was observed, especially up to 3·0 kHz. This agreement means that the impact force time history determined using the small end acceleration can be reasonably used as a baseline to assess the force obtained by using Reynolds' theory and the lumped parameter model presented.

C. Impact force determination with the 8-d.o.f. lumped parameter system. The impact force spectrum was also obtained using the 8-d.o.f. lumped parameter system previously

presented (see Figure 9). The energy method was used to set-up the system of equations [29], which was reduced to 7-d.o.f. when θ_1 was locked. The elements of these matrices were previously determined and the only unknown parameter is the damping factor (*Co*). Using the general form of the dynamic equilibrium system shown below, it was possible to obtain three expressions where the oil's effective damping factor could be isolated.

$$[K]\{x\} + [C]\{\dot{x}\} + [M].\{\ddot{x}\} = \{f\}.$$

The expression obtained to determine *Co* is

$$Co = \left[\frac{\phi_1 Ks + \dot{\phi}_1 Cs + \ddot{x}_4 Ms\, Scg + \ddot{\phi}_1(Is + Ms\, Scg^2)}{(\dot{x}_3 - \dot{x}_4 - \dot{\phi}_1 Lsi)Lsi}\right]. \tag{11}$$

The parameters $\ddot{x}_3, \ddot{x}_4, \ddot{\phi}_1$ and $\ddot{\phi}_2$ are obtained from the measured quantities *acw*, *ase, ads* and *ats* (Figure 8), respectively. The velocity and displacement vectors are obtained by integrating the acceleration vector once and twice respectively.

The start of the impact was considered to be at the moment when the acceleration *ads* crosses zero at time *ti*. This signal is positive when the piston is under gravitational force only and suddenly changes direction when the oil film starts to be squeezed. At this instant, all displacements have been considered equal to zero, which means that the integration constant for the displacements should have a value that brings them to zero at *ti*.

The acceleration time histories have shown that the velocities at the end of each impact, at time *tf*, were zero, except for the cylinder wall. In this case, the velocity is zero at *ti*, just at the start of the impact. Equation (11) was solved for each time step for each impact. The time history of the damping factor has been correlated with the film thickness by the expression $Co_{(t)} = Kh(t)^{\alpha}$. The coefficients K and α were obtained by using the least squares method. Table 1 presents these coefficients for five impacts and four different piston angles, and also the exponentially averaged results of K and α. The oil film thickness is in micrometre (m).

The results presented in Table 1 show that the effective damping factor is inversely proportional to the thickness cubed, as expected from Reynolds' equation, it shows also that factor K is different for each angle. The impact force time history has been calculated by multiplying the effective damping factor by the oil film squeeze velocity (vs), as follows:

$$Fo(t) = Co(t)vs(t) \quad \text{or} \quad Fo(t) = Kh(t)^{\alpha}vs(t), \tag{12}$$

TABLE 1

Coefficients K and α for different impact configurations

Impact test	Angle –0·14 (deg)		Angle –0·07 (deg)		Angle 0·00 (deg)		Angle 0·04 (deg)	
	$K \times 10^9$	α	$K \times 10^9$	α	$K \times 10^9$	α	$K \times 10^9$	α
1	3·173	−3·237	1·265	−2·850	6·558	−3·666	0·438	−2·96
2	3·753	−2·911	2·194	−3·252	5·819	−3·560	1·391	−3·206
3	6·978	−3·035	3·693	−3·336	9·454	−3·420	3·266	−3·137
4	44·88	−3·321	1·427	−2·865	0·654	−2·900	5·132	−2·924
5	22·86	−3·372	14·11	−3·523	29·00	−3·400	3·050	−3·245
Average	9·68	−3·17	21·79	−3·16	22·49	−3·39	2·14	−3·09

The squeeze velocity can be derived from the velocities $\dot{x}_3, \dot{x}_4$ and $\dot{\phi}_1$ or from the displacements dsp_1 and dsp_2. It has been assumed that $h(t)$ is the minimum film thickness over the skirt at any instant. The velocity $vs(t)$ has also been calculated for this minimum point. Figures 19 and 20 present some time histories of the calculated impact forces using equation (12). These figures also show the impact force calculated by multiplying the piston's effective mass by the small end acceleration (*ase*). For some impacts there is a discrepancy between the force calculated by this method and that obtained using *ase*. These disagreements may be caused by uncertainty of the experimental measurements, errors on the piston skirt and cylinder wall profile, consideration of θ_1 as locked, etc.

D. Impact force determination by using Reynolds' theory. The force time histories obtained by using Reynolds' theory have been compared with the forces obtained by using the small end acceleration. The results of eight different impact configurations are

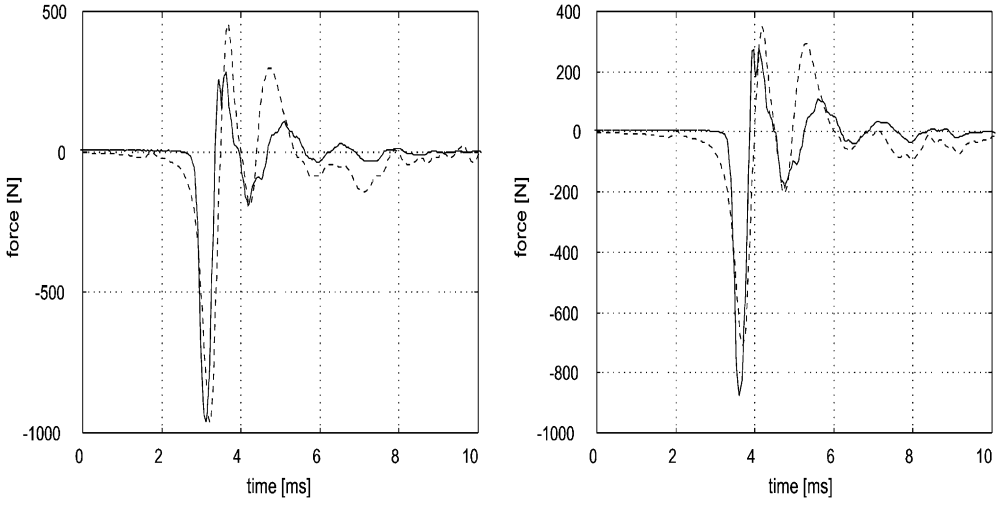

Figure 19. Impact force for the angle of $-0{\cdot}14^\circ$ derived from the lumped parameter model (- - - -) and from the small end acceleration (——), repeated two times.

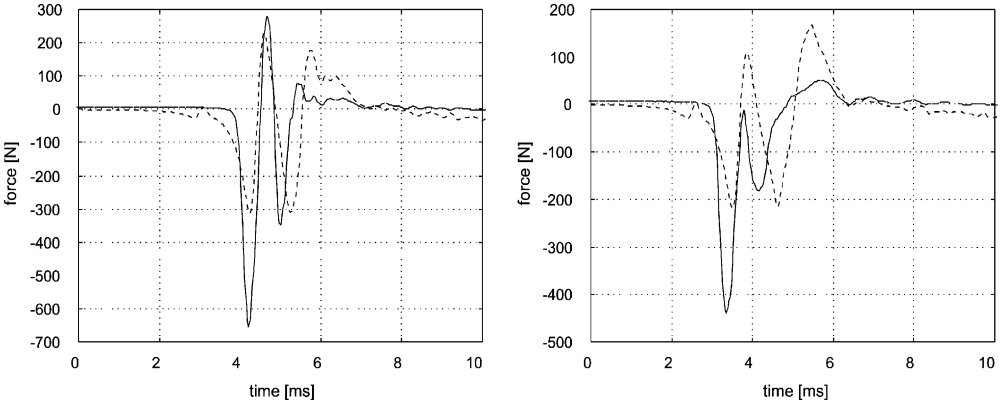

Figure 20. Impact force for the angle of $+0{\cdot}04^\circ$ derived from the lumped parameter model (- - - -) and from the small end acceleration (——), repeated two times.

presented in Figures 21 and 22, for piston angles of $-0{\cdot}14$ and $+0{\cdot}04^\circ$ and four repetitive trials each, respectively. The results show that the ratio between the forces obtained by these two methods is proportional again to the impacting velocity, initial oil film and a form factor. The same situation was found in the first test rig, where the trapped air influenced the impact force amplitude [27, 28]. The ratio factor is defined here as

$$ratio = C(\theta) vi \, e^{\beta(\theta) hi}, \tag{13}$$

where ratio peak (force Reynolds)/peak (force *ase*), $C(\theta)$ and $\beta(\theta)$ are the coefficients to be determined, vi, is the piston velocity at ds_2 (m/s), hi the oil film thickness at ds_2 (μm), and θ the piston locking angle (rad).

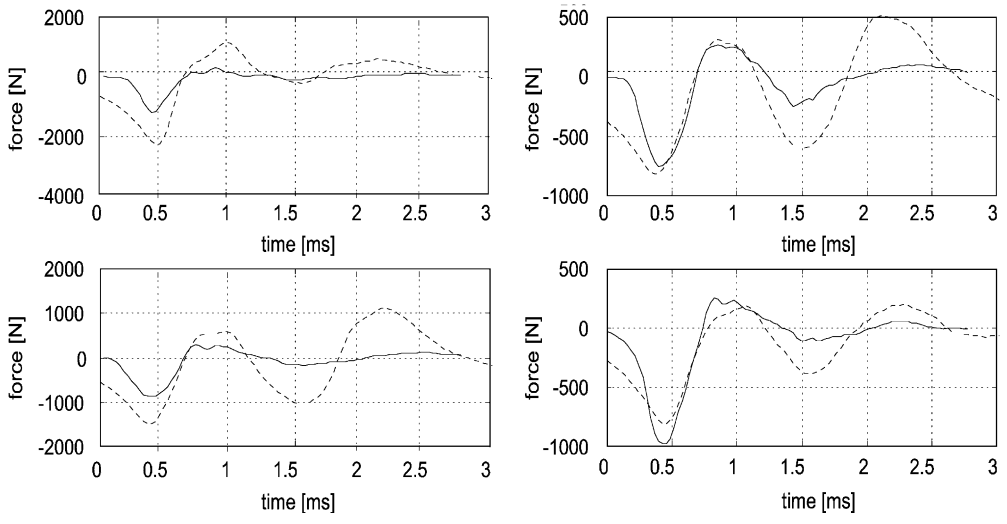

Figure 21. Impact force for $-0{\cdot}14^\circ$ obtained by using the integration routine (- - - -) and derived from the small end acceleration (——), repeated four times.

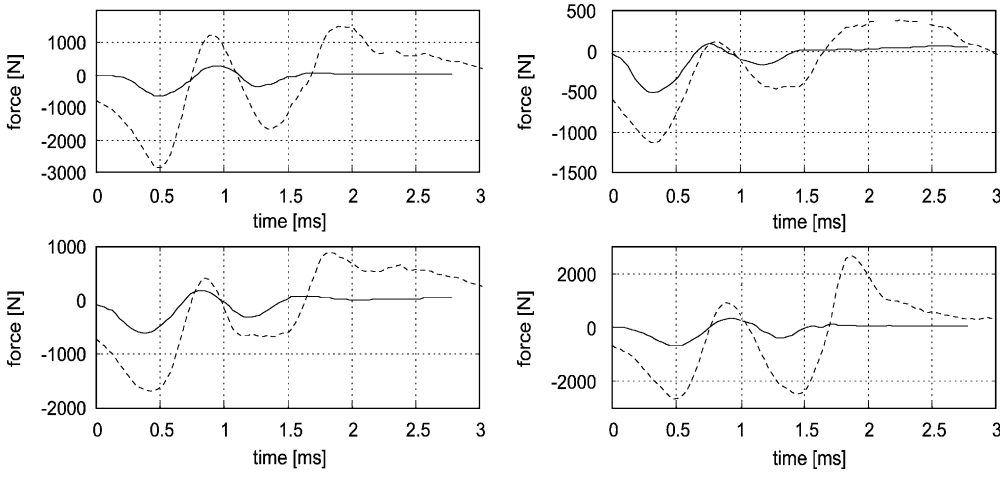

Figure 22. Impact force for $+0{\cdot}04^\circ$ obtained by using the integration routine (- - - -) and derived from the small end acceleration (——), repeated four times.

The form factor will depend on the geometrical configuration of each impact, e.g., on the form of the piston skirt and cylinder and on the piston's angle. Coefficients $C(\theta)$ and $\beta(\theta)$ were determined for each piston angle using the same procedure employed in the first rig. The initial oil film thickness and impacting velocity were derived from the measured displacements (Figure 8). Table 2 presents coefficients $C(\theta)$ and $\beta(\theta)$ determined for each piston angle. An average of 11 peak forces of different impact configurations was used to determine these coefficients. The correlation for each curve fitting was $-0{\cdot}9$, $-0{\cdot}7$, $-0{\cdot}9$ and $-0{\cdot}8$ for angles of $-0{\cdot}14$, $-0{\cdot}07$, $0{\cdot}00$ and $+0{\cdot}04^\circ$, respectively.

The results presented in Table 2 have been fitted again using a second degree least-squares method routine. The result for this fitting is

$$C(\theta) = 759 + 6{\cdot}686(10^5)\theta + 174(10^8)\theta^2,$$
$$\beta(\theta) = -0{\cdot}0234 - 7{\cdot}544\theta - 1{\cdot}525\theta^2. \tag{14}$$

Substituting $C(\theta)$ and $\beta(\theta)$ into equation (13) gives

$$ratio = (759 + 6{\cdot}686(10^5)\theta + 1{\cdot}74(10^8)\theta^2)vi\, e^{(-0{\cdot}0234-7{\cdot}544\theta-1{\cdot}525\theta^2)hi}. \tag{15}$$

Figures 23 and 24 show the same series as Figures 21 and 22 after correcting the force using equation (15). These figures show that the ratio factor obtained from equation 15 can be used with confidence to correct the force obtained from the integration routine.

TABLE 2

Coefficients $C(\theta)$ and $\beta(\theta)$ for different impact configurations

Angle $-0{\cdot}14$ (deg)		Angle $-0{\cdot}07$ (deg)		Angle $0{\cdot}00$ (deg)		Angle $+0{\cdot}04$ (deg)	
$C(\theta)$	$\beta(\theta)$	$C(\theta)$	$\beta(\theta)$	$C(\theta)$	$\beta(\theta)$	$C(\theta)$	$\beta(\theta)$
132·7	$-1{\cdot}37$	354·4	$-1{\cdot}78$	550·2	$-2{\cdot}16$	1415	$-3{\cdot}03$

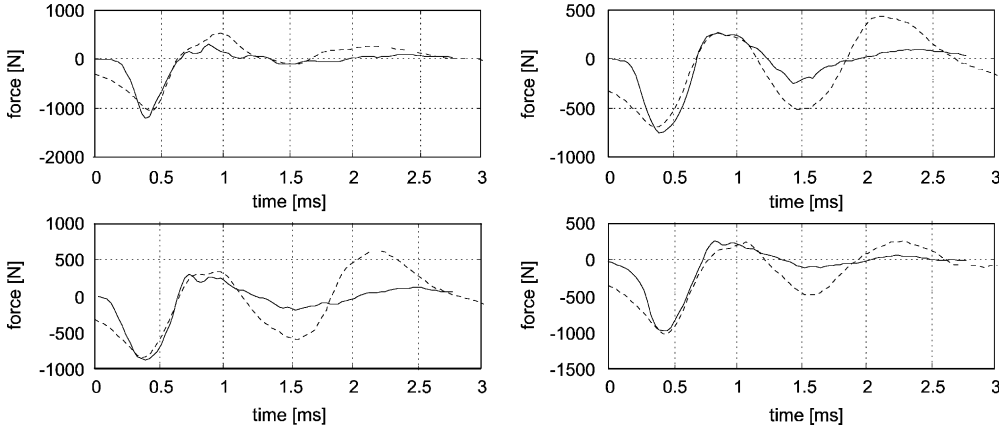

Figure 23. Impact force for $-0{\cdot}14^\circ$ using the integration soft (- - - -) corrected by equation (6), and derived from the small end acceleration (—), repeated four times.

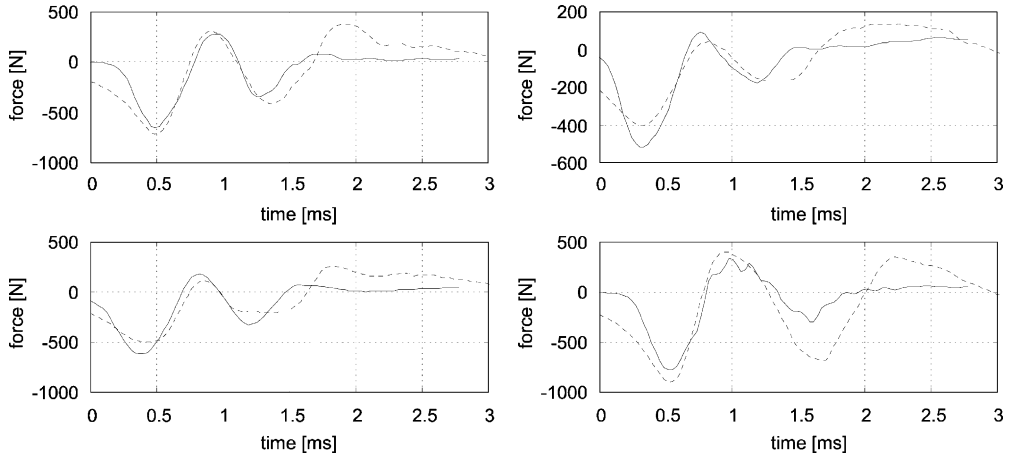

Figure 24. Impact force for $+0{\cdot}04^{\circ}$ using the integration soft (----) corrected by equation (6), and derived from the small end acceleration (——), repeated four times.

4. PISTON SLAP MODEL VALIDATION IN A MOTORED ENGINE—STAGE III

The first and second test rigs allowed the study of oil film effects on the behaviour of impact between two rigid bodies and between the piston and the cylinder wall respectively. Four methodologies were used in the second rig to determine the impact force. These methodologies have also been used to determine the impact force in a motored engine (a more realistic approach), where there is a variation of the oil film temperature and of the level of the impact force.

A third test rig was set-up for performing the experimental tests on a fully assembled engine and to determine the piston slap time history. This rig comprises a motoring facility powered by an electric motor that drives an instrumented internal combustion engine (same engine model as used in the second rig). This engine was assembled in two different configurations, i.e., without any valves (inlet and exhaust), and secondly the inlet and exhaust valves were refitted to cylinder #2. For each configuration, different tests were performed with the engine motored at speeds of 2500, 3000, 3500 and 4000 r.p.m. A dynamic model was proposed to simulate the oil film mixed with gas bubbles and the correction factor (ratio) could be estimated by using this model.

Although this rig is not completely representative of a running internal combustion engine, especially in terms of thermal signatures, nevertheless it is quite sufficient for the developing and validating the oil film model. The motored engine also had the advantage that, since temperatures were much lower than when it was running normally, thermal distortion of the piston was likely to be small. Hence, the measured cold profile could be reasonably assumed without significant error. Of course, with the running engine, the changed profiles of both the piston and the cylinder (calculated using FE models) would have to be taken into account.

4.1. TEST RIG SET-UP

The engine was assembled on stands inside an acoustic chamber to avoid the background noise from the electric motor and drive assembly. The parameters necessary to calculate the impact force in the second rig are the acceleration of the small end,

cylinder wall, skirt and a point on the block panel, as well as the displacement of the piston in two positions. However, in a motored engine some of these values, such as the acceleration of the small end and skirts, could not be measured without special instrumentation.

Therefore, the following parameters were measured: cylinder wall acceleration, engine block acceleration at a specific external point, piston skirt displacement at two points, engine speed, cylinder pressure and sound pressure level at two points inside the acoustic chamber. This test rig was divided into the following sub-systems.

4.1.1. *Mechanical sub-system*

This mechanical sub-system is responsible for generating piston slap when the engine is motored at different speeds. It consists of the following parts.

The motoring facility. The motoring facility comprises a variable-speed electric motor and a driving system which enables the engine to be motored at different speeds: manufacturer: ASEA FULLER, type, KB24; power: 42/44 hp; speed, 167–1670 r.p.m.

The drive system consists of the drive shafts and belts and an electro-mechanical clutch. A set of pulleys is used to drive and multiply the speed generated by the electric motor. The electro-mechanical clutch is coupled to the main shaft to control and smooth the power engagement between the driving system and the engine.

The Internal Combustion Engine (ICE). The engine used is a four-cylinder in-line, four-stroke, overhead camshaft, compression ignition unit of 1·81 (Figure 25): manufacturer: FORD; engine code: RTC/RTD; bore 82·5 mm; stroke: 82·5 mm; maximum power: 60 bhp (DIN) at 4800 r.p.m; maximum torque: 110 Nm at 2500 r.p.m.

4.1.2. *Acoustic chamber*

The motoring facility was assembled outside the acoustic chamber where the engine was set-up. This chamber is a simple acoustically isolated room with an independent floor, and has the dimensions of 3·75 m width, 3·15 m length and 2·36 m height. The walls and roof are treated with 100 mm rockwool acoustic absorption. The reverberation time of the chamber was measured in octave bands from 32·5 to 8000 Hz. It was observed that the absorption factor for frequencies above 250 Hz is higher than 80%.

4.1.3. *Instrumentation and their metrological characteristics*

The engine was instrumented with two accelerometers (B&K 4375), two displacement sensors (KAMAN KD 2300 0·5 SU), two temperature sensors, one pressure transducer and one crank-shaft speed pick-up. Two microphones and one trigger probe were also used. One accelerometer (*acw*) was fixed to the waterside of the thrust side of the cylinder wall. The other accelerometer (*abl*) was fixed at a defined point on the outer surface of the engine block. One non-contact displacement sensor was fitted at the top of the cylinder (ds_1) and other at the bottom (ds_2), to measure the top skirt and bottom skirt displacements, respectively. The positions of these sensors were calculated to measure displacements when the piston is at top dead centre (TDC) $\pm 20^\circ$, which is the most common range where main piston slap takes place in a running engine. One thermocouple type *K* was fixed to the waterside of the cylinder wall and the other fixed to the outer surface of the oil sump, with a maximum error of $\pm 2^\circ$C over 0–100°C. One pressure transducer (*pt*) KISTLER 601A was fitted in the place of the fuel injector in the pre-chamber of cylinder 2, and its signal conditioned by a KISTLER 5007 charge amplifier (operational range of 0–25·3 MPa, with a maximum error of 0·5%). A pulse counter was

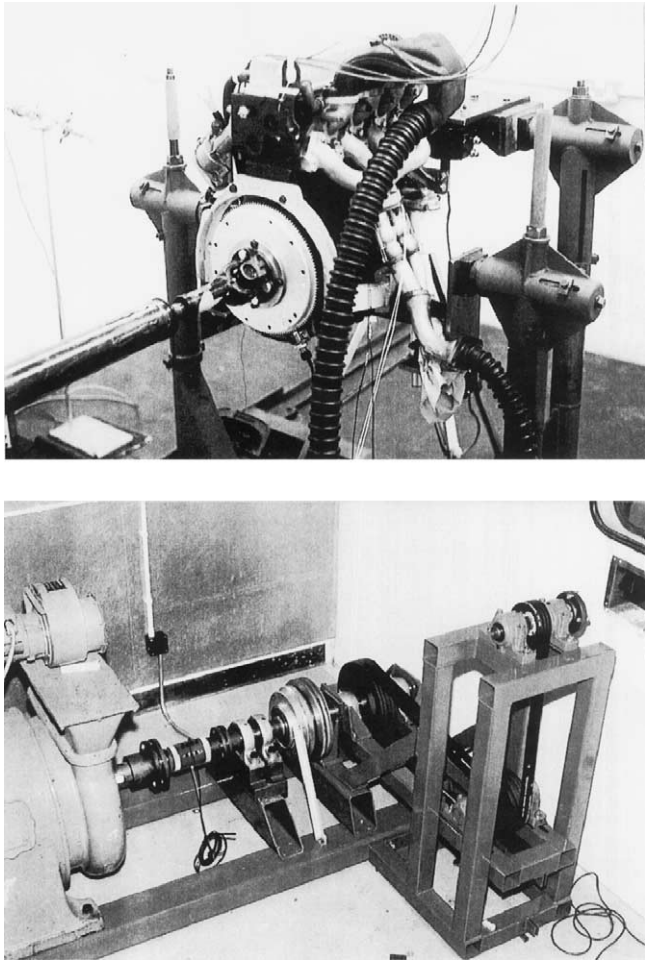

Figure 25. Motoring facility (views of different parts).

fixed close to the front pulley of the crank-shaft to measure the engine speed ± 20 r.p.m. Two calibrated microphones B&K 4165 were positioned at 1 m from the thrust side (μp_1) and 1 m from the anti-thrust side (μp_2) of the engine. A Hewlett–Packard HP3566A was used to perform the data acquisition of eight channels simultaneously.

When the engine was assembled without valves, only the inertia forces of the reciprocating mechanism generated piston slap. This configuration was adopted to avoid the engine warming up too quickly, since the engine was assembled without a cooling system. Four kinds of tests were carried out using this configuration, with the data acquisition commencing with the engine: (1) cold and the speed increasing from 2500 to 4000 r.p.m in steps of 500 r.p.m.; (2) cold and the speed decreasing from 4000 to 2500 r.p.m. in steps of 500 r.p.m.; (3) warmed-up and the speed increasing from 2500 to 4000 r.p.m. in steps of 500 r.p.m.; (4) cold and the speed fixed at 3000 r.p.m, until fully warmed-up.

Because the engine was motored without a cooling system, the temperature rose quickly up to 90°C, when it stabilized.

After proceeding with the tests for the engine without compression, the inlet and exhaust valves were refitted to cylinder 2. With this configuration the motored engine behaviour is quite similar to the running engine, with the pressure in the chamber being quite high (peak pressures in the order of 5·5 MPa were measured). In this case, the slaps are generated by the inertia forces and by the air pressure in the cylinder. Two tests were carried out using this configuration, with the engine started: (1) cold with the speed increasing from 2500 to 4000 r.p.m. in steps of 500 r.p.m.; (2) cold with the engine speed fixed at 3000 r.p.m. until fully warmed-up.

It was verified that the cylinder wall temperature did not rise very fast because the compression occurred in only one cylinder and the thermal inertia of the rest of the engine dissipated the heat. In some tests this temperature reached the limit of 100°C.

4.2. TRANSFER FUNCTION MEASUREMENTS

Two transfer functions were measured on the engine block after it was assembled on its stands. These transfer functions were used to calculate the impact force spectrum as described for the second test rig. The cylinder head was removed and one accelerometer was fixed on the inner side of the cylinder wall at the same position as *acw*, and the drive point inertance (dp_1) was obtained by hitting the waterside of the cylinder wall with an instrumented hammer. The transfer function (tf_{12}) between the cylinder wall at *acw* and the point on the block panel (*abl*) was obtained by hitting this point and dividing the output acceleration of *acw* by the input force.

4.3. PISTON MOVEMENT DETERMINATION

Because the displacement sensors are fitted in the cylinder wall and the piston is moving, the sensors measure the oil gap over the skirt at different points during the piston movement. The measured gap is considered to be filled by oil. Considering that the piston can only slide up and down and rock around its gudgeon pin, a simple geometrical formulation can be used to determine the oil film thickness over the whole skirt (as in the second rig) from these two known gaps.

4.4. MODEL FOR THE LUBRICANT OIL MIXED WITH AIR BUBBLES

The results of the first two rigs showed that the trapped air can strongly affect the level of the force calculated by using Reynolds' equation, and a ratio factor was defined for correcting this force. In those cases, the temperature was fixed and the air was pushed into the oil film in a repetitive way that depended on the form and relative velocity of the impacting surfaces. In the third rig, the piston skirt is lubricated by the oil being pumped from the sump to the cylinder walls. Such a pumping process can also trap air in the oil, and this can be easily verified by just observing the bubbles on the dipstick of a running engine.

A model has been proposed to determine the dynamic behaviour of an oil film contaminated by air bubbles (Figure 26). This model can be used to determine the ratio factor for correcting the force calculated using Reynolds' theory and to understand how the lubricating film behaves when it contains trapped air bubbles [27–29].

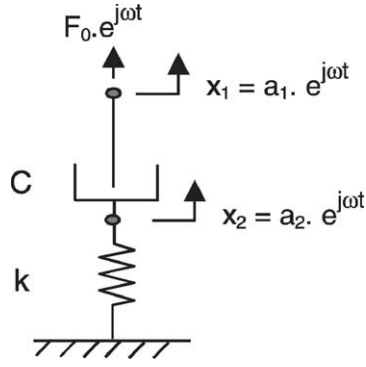

Figure 26. Model for the oil film with trapped air.

The formulation for this model is presented below:

$$F_0 e^{j\omega t} = C(\dot{x}_1 - \dot{x}_2) = kx_2, \quad F_0 = j\omega C(a_1 - a_2) = ka_2,$$

$$j\omega C a_1 = a_2(k + j\omega C),$$

$$F_0 = j\omega C a_1 \left(1 - \frac{j\omega C}{k + j\omega C}\right) = j\omega C a_1 \left(\frac{k}{k + j\omega C}\right),$$

$$F_0 = C\omega a_1 jk \left(\frac{k - j\omega C}{k^2 + (\omega C)^2}\right) = \frac{C\omega a_1 k}{k^2 + (\omega C)^2}(jk + \omega C),$$

$$|F_0| = \frac{C(\omega a_1)k}{(k^2 + (\omega C)^2)}\sqrt{k^2 + (\omega C)^2} = |F_0| = \frac{Ck(\omega a_1)}{\sqrt{k^2 + (\omega C)^2}}. \tag{16}$$

Equation (16) shows the relation between the impact force (*Fo*) and the damping factor of the oil film and the stiffness introduced by the bubbles. Based on this equation, the following observations can be made:

(1) Considering the oil damping factor (viscosity) constant, which is the case for the two first rigs, two limiting conditions apply: (a) when k is very large, there are no or very few bubbles; therefore, $|Fo| \cong C(\omega a_1)$, which follows Reynolds' equation, since (ωa_1) is the velocity. Thus the impact is dominated by the damping; (b) when k is very small, i.e., there are many bubbles; therefore, $|Fo| \cong ka_1$, and the impact is dominated by the bubbles (low stiffness).
(2) Considering the stiffness (quantity of the air bubbles) constant, two possible limiting conditions apply: (a) at high temperature when the viscosity is low, e.g., $\omega C = k$ the force $|Fo| \cong C(\omega a_1)/2^{1/2}$, which means that the force obtained by Reynolds is divided by a factor of $2^{1/2}$ (correcting ratio); (b) at low temperature, when the viscosity is high, e.g., $\omega C = 10k$, the force $|Fo| \cong C(\omega a_1)/101^{1/2}$, which means that the force obtained by Reynolds is divided by a factor of $101^{1/2}$.

The ratio factor can be derived from this model. Consider that there is a relation such as $\omega C = \alpha k$, where α is a coefficient that depends on the quantity of trapped air. In this case, the ratio factor can be written as

$$ratio = \frac{\sqrt{k^2 + (\omega C)^2}}{k} \sqrt{1 + \alpha^2}.$$

The damping factor can be defined as $C = \beta\eta$, where β is a factor depending on the film thickness, impact velocity and geometry of the surfaces, and is considered as constant for the purpose of this analysis. Two situations are considered:

Case 1: Oil film at high temperature (t_H), thus η is low. If the ratio factor (ra_{tH}) is known for this situation,

$$\alpha = \sqrt{ra_{t_H}^2 - 1}, \quad \alpha = \frac{\omega C}{k} \frac{\omega}{k} \beta\eta_H.$$

Case 2. The oil film temperature is low (t_L), and how the bubbles are entrapped and their quantity are fairly repetitive. The viscosities η_L and η_H are obtained from the viscosity equation presented in equation (8),

$$\frac{\eta_L}{\eta_H} = \frac{C_L}{C_H} = \frac{\alpha_L k/\omega}{\alpha_H k/\omega} \quad \Rightarrow \text{known},$$

$$\frac{\alpha_L}{\alpha_H} = \frac{0{\cdot}95\mathrm{e}^{-0{\cdot}057T_L}}{0{\cdot}95\mathrm{e}^{-0{\cdot}057T_H}} = \mathrm{e}^{0{\cdot}057(T_H - T_L)},$$

$$ra_L = \sqrt{1 + (ra_H^2 - 1)\mathrm{e}^{0{\cdot}114(T_H - T_L)}}. \tag{17}$$

Equation (17) shows that there is a relation between the ratios for different oil temperatures when the stiffness factor is constant (quantity of mixed air). The measured data were processed and the impact behaviour analyzed to determine the impact force time history for different operational regimes of the engine.

4.5. IMPACT FORCE TIME HISTORIES

The impact force was determined by using three different methods, as follow

A. Determination of the impact force by integrating Reynolds' equation. The oil film thickness was determined over the piston skirt as described previously. The time history of the oil film distribution is used together with other parameters to integrate Reynolds' equation and determine the squeeze force F_{re}, which was calculated for the tests executed in the engine with valves, i.e., with compression. Figure 27 shows the impact force time histories for the engine started cold and the speed varying from 2500 to 4000 r.p.m. Figure 28 shows the time histories for the engine started cold and at a fixed speed of 3000 r.p.m. At the right side of each graph there is the cylinder wall temperature *tcw* (considered the same as the oil film) and the corresponding engine speed.

B. Impact force spectrum derived from the transfer functions. The impact force spectrum can be determined by dividing the cylinder wall acceleration (*acw*) spectrum (caused by the piston impact) by the transfer function (dp_1). This assumes that the piston impacts at the point on the cylinder where the transfer function was measured. In fact, it was observed that the drive-point inertia is practically the same along the cylinder wall, therefore, a good estimate of the impact force spectrum can be achieved.

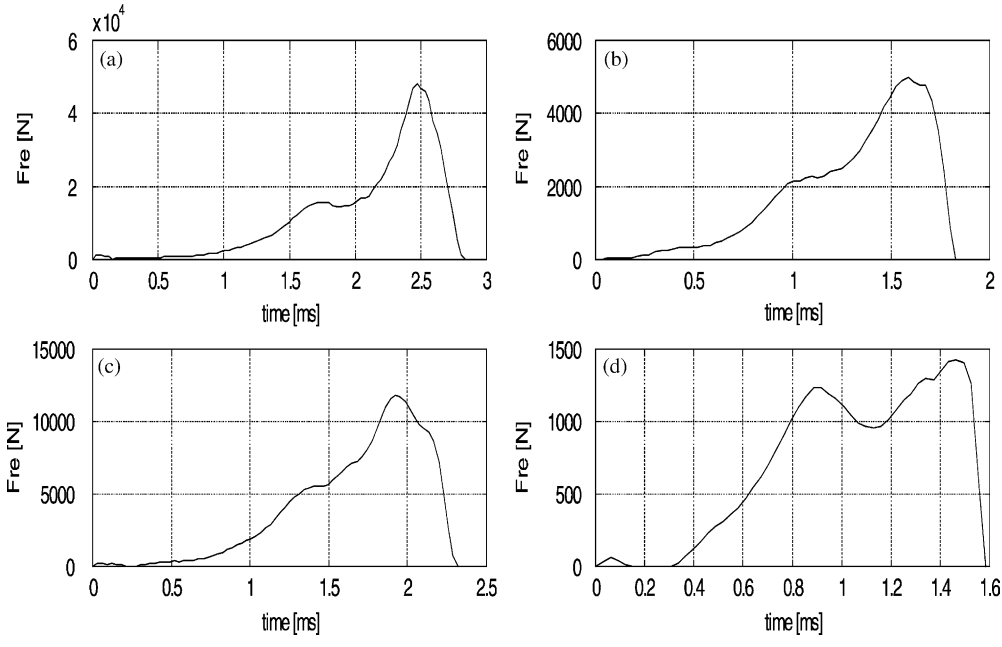

Figure 27. Impact force time histories determined using Reynolds' theory: (a) 2500 r.p.m., *tcw* 32°C, (b) 3500 r.p.m., *tcw* = 64°C; (c) 3000 r.p.m, *tcw* = 46·8°C, (d) 4000 r.p.m., and 82°C.

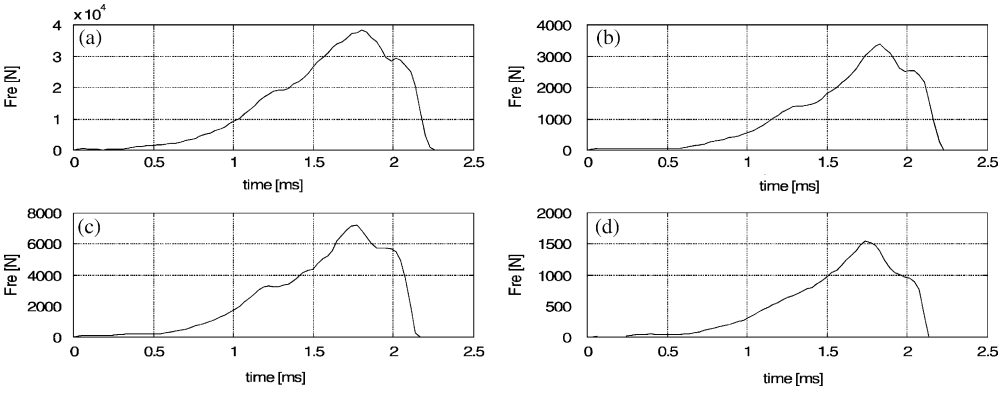

Figure 28. Impact force time histories determined using Reynolds' theory: (a) 3000 r.p.m., *tcw* = 30°C, (b) 3000 r.p.m., *tcw* = 63·3°C, (c) 3000 r.p.m., *tcw* = 75°C, and (d) 3000 r.p.m., *tcw* = 85°C.

C. Determination of the impact force using lateral piston acceleration. The piston acceleration was determined by double differentiation of the measured displacements, after smoothing treatment. The piston effective mass (*Mr*) is multiplied by lateral acceleration (*ase(t)*) to estimate the impact force. This procedure can estimate the piston's lateral force of inertia and is an approximation because it assumes that the piston acts as a rigid body [4] and neglects any rotational component in the piston's motion. To determine the impact force ($Fsq(t)$) it is necessary to include the con-rod's side force ($SF(t)$), and the final equation is: $F_{sq}(t) = SF(t) + Mr\,ase(t)$.

Figure 29 shows a time history for force F_{sq} and for the force calculated using Reynolds' equation (F_{re}) with a high cylinder wall temperature. It is observed that there is a relatively good agreement between the time histories of the forces F_{sq} and F_{re}. Figure 30 shows force spectra calculated by all three methods just described, where the engine was started cold and the speed varied from 2500 to 4000 r.p.m. Figure 31 shows these three force spectra for the engine at a fixed speed of 3000 r.p.m., where the engine was started cold and was then warmed-up.

4.6. ANALYSIS OF THE IMPACT FORCE TIME HISTORIES

Figures 27 and 28 show the impact force time histories obtained using Reynolds' theory considering the oil without air bubbles. In this case, it is observed that the force levels are very high at low temperatures. These time histories showed that the impact occurs in two parts. First the bottom skirt approaches the cylinder wall and a reaction force is applied by the oil film which rocks the piston about the gudgeon pin. The following movement squeezes the oil towards the top skirt until the maximum reaction force takes place and pushes the piston towards the anti-thrust side. Figures 30 and 31 show that for low temperatures there is a large discrepancy between the spectra obtained using the transfer function method and Reynolds' equation. As suggested by the oil film model previously presented, this discrepancy considerably reduces when the temperature rises (viscosity reduces). The spectrum of F_{11} is adopted as baseline to compare the impact forces because it is derived from acceleration *acw*, which is mostly caused by the impact of the piston in the cylinder considered, and the drive-point function dp_1. Table 3 compares the measured and theoretical ratios between the spectra of the forces F_{re} and F_{11}. The measured ratio is

$$ratio = 20 \log\left(\frac{\sum F_{re}}{\sum F_{11}}\right), \tag{18}$$

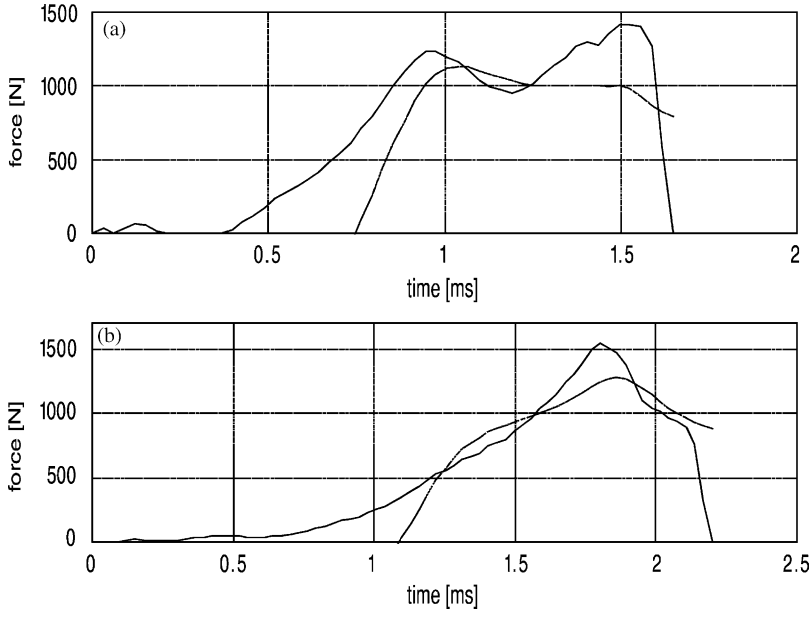

Figure 29. Impact forces obtained using Reynolds' equation (F_{re}) and the small end acceleration (F_{sq}): (a) 4000 r.p.m. $tcw = 82°C$; (b) 3000 r.p.m, $tcw = 85°C$.

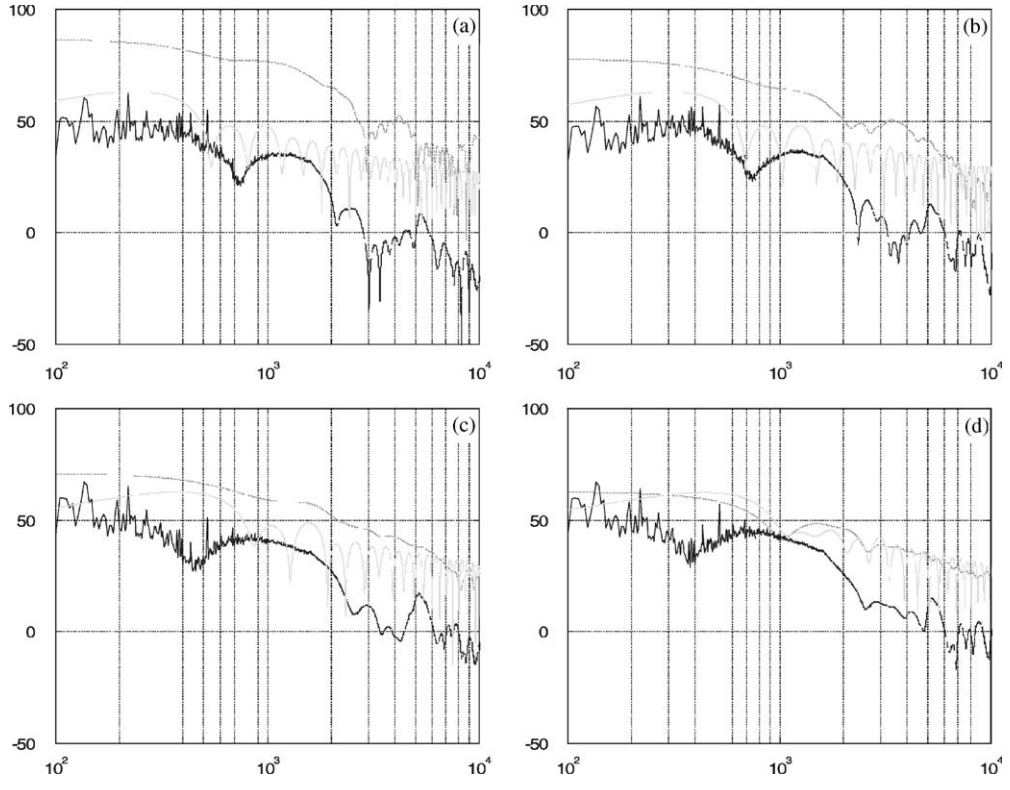

Figure 30. Force spectra for the engine at (a) 2500 r.p.m. and $tcw = 32{\cdot}0°C$, (b) 3000 r.p.m. and $tcw = 46{\cdot}8°C$, (c) 3500 r.p.m. and $tcw = 64{\cdot}0°C$ and (d) 4000 r.p.m. and $tcw = 82{\cdot}0°C$. Lower bold solid curve obtained by transfer function measurements (see sections 4·2 and 4·5(B)), middle faint dotted curve obtained from piston movement determination (see sections 4·3 and 4·5(C)), and upper faint curve is calculated from Reynold theory (see sections 4·4 and 4·5(A)).

where $\sum F_{re}$ is the sum of the F_{re} amplitudes from 100 to 10 000 Hz, and $\sum F_{11}$ the sum of the F_{11} amplitudes from 100 to 10 000 Hz.

It can be seen that the theory predicts the ratio accurately although it should be noted that, since equation (18) only gives relative values, the ratio has been normalized to the condition related to Figure 31 with the oil film at 85°C (Case 'd').

5. CONCLUSIONS

Experimental tests were extensively carried out using three specially designed test rigs and good agreement between predicted and measured piston slap impact forces was obtained. The first rig allowed a better understanding of the influence of the oil film on the impact phenomenon, and the applicability of Reynolds' equation for oil squeezing under impacting conditions was demonstrated. An analytical expression was derived from the Reynolds' equation for calculating the impact force.

The experimental results of the first rig showed that when air is trapped in the oil film, the measured force can be much lower than that predicted by the theory.

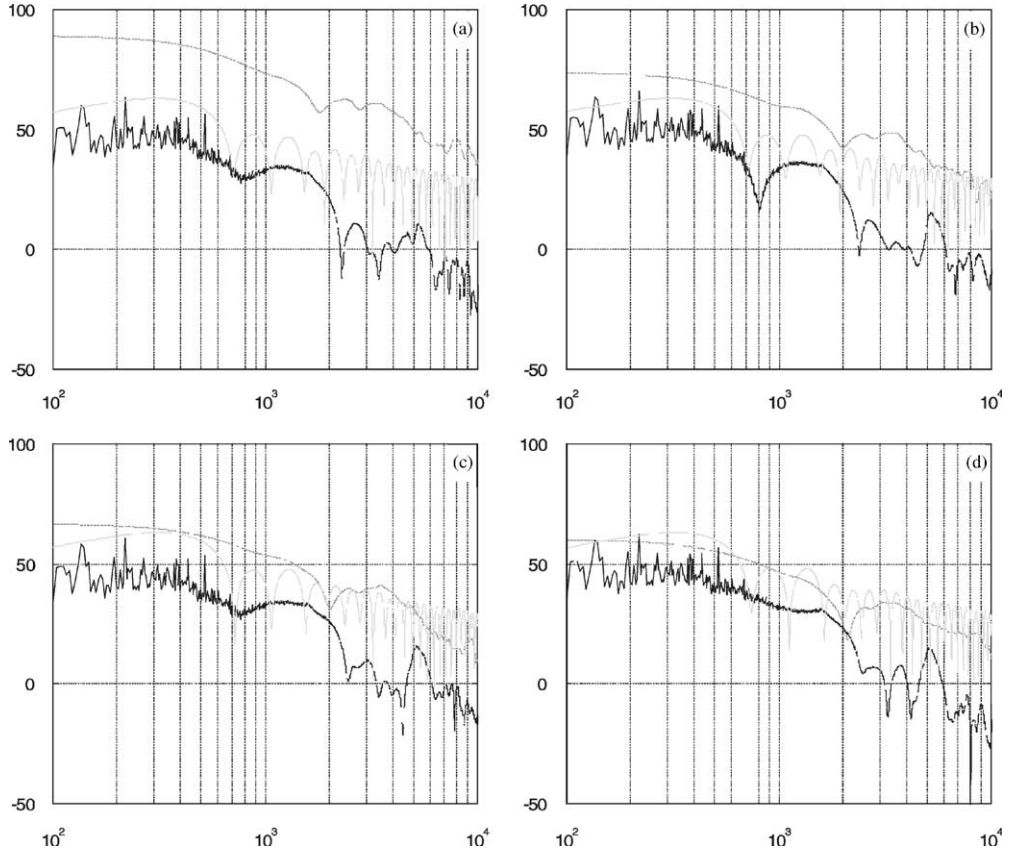

Figure 31. Force spectra for the engine at 3000 r.p.m. and (a) $tcw = 30{\cdot}0^\circ$C, (b) $tcw = 63{\cdot}3^\circ$C, (c) $tcw = 75{\cdot}0^\circ$C and (d) $tcw = 85{\cdot}0^\circ$C. Lower bold solid curve obtained by transfer function measurements (see sections 4·2 and 4·5(B)), middle faint dotted curve obtained from piston movement determination (see sections 4·3 and 4·5(C)), and upper faint curve is calculated from Reynold theory (see sections 4·4 and 4·5(A)).

TABLE 3

Ratio between F_{11} and F_{re}

Engine condition	Test	Measured ratio in (dB)	Ratio predicted by equation (18) (dB)	Oil film temperature (°C)
Figure 30	A	36	35	32
	B	27	27	47
	C	21	19	64
	D	10	10	82
Figure 31	A	38	37	30
	B	23	21	64
	C	16	15	75
	D	10	10	85

The second rig allowed a better study of the impact between the piston and the cylinder wall of an internal combustion engine. Reynolds' equation was solved using the finite difference method and again it was found that the bubbles generated during the impact greatly affected the impact force as calculated using Reynolds' equation.

A dynamic model comprising a spring (air bubbles) connected to a dashpot (oil film) in series was proposed to simulate the oil film behaviour mixed with air bubbles. The model could predict the trend of the ratio between the effective viscosity of the oil and air bubble mixture to the pure oil viscosity. It was observed that as the oil temperature rises and its viscosity decreases, even mixed with bubbles, Reynolds' theory gives better agreement with the measured force.

The third test rig was used to evaluate the proposed assessment model and extensive experimental tests have shown that this model can be used for predicting the impact force time history.

It should be emphasized that the theory of Reynolds for fluid squeezing can be used for impact force determination. Nevertheless, it is quite important to ensure that the fluid is not contaminated by air bubbles and, if it is, a spring–dashpot model is highly recommended for better results.

Future works can consider the effects of thermal paths and temperature effects on the piston in the real engine. Also the effect of the stiffness of the connecting rod on the dynamics of the piston slap should be studied.

ACKNOWLEDGMENTS

This work reports the main results of a thesis research project sponsored by CAPES (Brazilian Council of Technology) and carried out at the Vehicle Dynamics Group, Institute of Sound and Vibration Research of University of Southampton/England and the Mechanical Engineering Department of Federal University of Santa Catarina/Brazil.

REFERENCES

1. J. J. Toulmin 1996 *Vehicle Environmental Legislation: Past, Present and Future, Collected Papers from the One-day Seminar*. '*The Tribology of Internal Combustion Engines*', University of Birmingham, pp. 1–8, 7 November.
2. Resoluções CONAMA No. 1 e 2/93 1993 *Limites de Emissão de Ruídos por Veículos Automotores*, Brazil.
3. J. L. L. Cavalcanti 1995 *Development and Refinement of a New Engine Family to Achieve Future Noise Legislation and Acoustic Driving Comfort Requirements*, IV Congresso e Exposicão Internacionais de Tecnologia da Mobilidade, São Paulo-SP, SAE 952292, 2–4 October 1995.
4. K. Ohta, Y. Irie, K. Yamamoto and H. Ishikawa 1987 *Piston Slap Induced Noise and Vibration of Internal Combustion Engines (1st Report, Theoretical Analysis and Simulation)*, SAE 870990, pp. 337–342.
5. M. Okubo, H. Kanda and T. Yonezawa 1989 *Analysis and Reduction of Piston Slap Noise in Diesel Engines*, *SAE* 890127. International Congress and Exposition, Detroit, MI, March.
6. T. Priede, J. Dixon, E. C. Grover and N. A. Saleh 1984 *Experimental Techniques Leading to the Better Understanding of the Origins of Automotive Engine Noise*. C151/84. Automotive Group — ISVR, Southampton University.
7. J. W. Slack 1983 *Proceedings NOISE-CON '83, Massachusetts Institute of Technology, Cambridge, MA*, 105–112. The mechanism of piston slap noise.
8. B. J. Challen and D. M. Croker 1982 *A Review of Recent Progress in Diesel Engine Noise Reduction*, *SAE* 820517. Detroit, U.S.A. pp. 1–32.
9. R. G. Dejong and N. E. Parsons 1982 *Piston Slap Noise Reduction in a Vee-Block Diesel Engine*, *SAE* 820240. pp. 93–101.
10. J. W. Slack 1982 *Ph.D. thesis, Massachusetts Institute of Technology*. February. Piston slap noise in diesel engines.
11. T. Priede 1982 In: *Noise and Vibration*, (R. G. White, editor). 391–437. Chichester, U.K.: Ellis Horwood Limited; Chapter 18.

12. N. Lalor, E. C. Grover and T. Priede 1980 *Engine Noise Due to Mechanical Impacts at Pistons and Bearings*, SAE 800402, February 25–29. ISVR, Congress and Exposition Cobo Hall, Detroit.
13. M. D. Rohrle 1975 *Affecting Diesel Engine Noise by the Piston*, *SAE* 750799.
14. T. Usami, S. Wada and S. Sonoda 1975 *Piston Slap Noise of Indirect Combustion Diesel Engine*, *SAE* 750801, pp. 80–88.
15. D. Ross and E. E. Ungar 1965 *On piston slap as a source of engine noise*, *ASME*, 65-OGP-10.
16. Z. Dursunkaya, R. Keribar and V. Ganapathy 1994 *Transactions of the American Society of Mechanical Engineers, Journal of Tribology* **116**, 777–785. A model of piston secondary motion and elastohydrodynamic skirt lubrication.
17. S. N. Y. Grges, J. C. Lca and N. Lalor 2000 *International Journal of Acoustics and Vibration* **5**, 37–45. A literature review of diesel engine noise with emphasis on piston slap.
18. J. P. Ryan 1993 *M.Sc. Dissertation, Massachusetts Institute of Technology*. Impact analysis of piston slap in a spark ignition engine.
19. D. Zhu, Y. Z. Hu, H. S. Cheng, T. Arai and K. Hamai, 1993 *Transactions of the American Society of Mechanical Engineers, Journal of Tribology* **115**, 125–133. A numerical analysis for piston skirts in mixed lubrication — Part II: Deformation considerations.
20. D. Zhu, H. S. Cheng, T. Arai and K. Hamai 1992 *Transactions of the American Society of Mechanical Engineers, Journal of Tribology* **114**, 553–562. A numerical analysis for piston skirts in mixed lubrication—Part I: basic modelling.
21. T. Konomi, M. Murakami and S. Sanda 1993 *Proceedings of the Institution of mechanical Engineers*, C465, 147–154. Effects of piston skirt profile on friction loss and oil film behaviour.
22. S. A. Hamad 1984 *M.Sc. dissertation, ISVR, University of Southampton*. Effect of oil film on engine mechanical impact and engine structure response.
23. K. T. Ewida 1982 *Ph.D. thesis*, *University of Southampton, ISVR*. A rheovibro study on the effect of an oil film on mechanical impacts.
24. F. Dennis, S. M. Rohde and H. A. Ezzat 1982 *ASLE Transactions* **26,** 151–160. An automotive piston lubrication model.
25. R. Gohar 1988 *Elastohydrodynamics*. Ellis Horwood Limited, John Wiley & Sons, ISBN 0-85312-820-0, pp. 59–78.
26. D. Dowson and G. R. Higginson 1966 *Elasto-hydrodynamic Lubrication*. Oxford: Pergamon Press Ltd; first edition, 1966.
27. S. Haber and I. Etsion 1985 *ASLE Transactions* **28**, 253–260. Analysis of an oscillatory film containing a central gas bubble.
28. H. Hashimoto 1995 *Transaction of the American Society of Mechanical Engineers, Journal of Tribology*, **117**, 513–518. Squeeze film characteristics between parallel circular plates containing a single central air bubble in the inertial flow regime.
29. J. C. De luca 1998 *Ph.D. Thesis, Universidade Federal de Santa Catarina, Brasil in agreement with University of Southampton—U.K.* September. The influence of cylinder lubrication on piston slap.
30. G. Tamai 1993 *Massachusetts Institute of Technology, Bachelor*, May. Data analysis of piston motion and engine block response characteristics in piston slap.